

2-2010

Arabidopsis RNA-Dependent RNA Polymerases and Dicer-Like Proteins in Antiviral Defense and Small Interfering RNA Biogenesis during *Turnip Mosaic Virus* Infection

Hernan Garcia-Ruiz

Oregon State University, hgarcia.ruiz2@unl.edu

Atsushi Takeda

Oregon State University

Elisabeth J. Chapman

Oregon State University

Christopher M. Sullivan

Oregon State University

Noah Fahlgren

Oregon State University, NFahlgren@danforthcenter.org

Follow this and additional works at: <http://digitalcommons.unl.edu/plantpathpapers>



Part of the [Other Plant Sciences Commons](#), [Plant Biology Commons](#), and the [Plant Pathology Commons](#)

Garcia-Ruiz, Hernan; Takeda, Atsushi; Chapman, Elisabeth J.; Sullivan, Christopher M.; Fahlgren, Noah; Bremmelis, Katherine J.; and Carrington, James C., "Arabidopsis RNA-Dependent RNA Polymerases and Dicer-Like Proteins in Antiviral Defense and Small Interfering RNA Biogenesis during *Turnip Mosaic Virus* Infection" (2010). *Papers in Plant Pathology*. 361.
<http://digitalcommons.unl.edu/plantpathpapers/361>

This Article is brought to you for free and open access by the Plant Pathology Department at DigitalCommons@University of Nebraska - Lincoln. It has been accepted for inclusion in Papers in Plant Pathology by an authorized administrator of DigitalCommons@University of Nebraska - Lincoln.

Authors

Hernan Garcia-Ruiz, Atsushi Takeda, Elisabeth J. Chapman, Christopher M. Sullivan, Noah Fahlgren, Katherine J. Bremmelis, and James C. Carrington

***Arabidopsis* RNA-Dependent RNA Polymerases and Dicer-Like Proteins in Antiviral Defense and Small Interfering RNA Biogenesis during *Turnip Mosaic Virus* Infection**

Hernan Garcia-Ruiz, Atsushi Takeda,¹ Elisabeth J. Chapman,² Christopher M. Sullivan, Noah Fahlgren, Katherine J. Brempeles, and James C. Carrington³

Center for Genome Research and Biocomputing, Department of Botany and Plant Pathology, Oregon State University, Corvallis, Oregon 97331

Plants respond to virus infections by activation of RNA-based silencing, which limits infection at both the single-cell and system levels. Viruses encode RNA silencing suppressor proteins that interfere with this response. Wild-type *Arabidopsis thaliana* is immune to silencing suppressor (HC-Pro)-deficient *Turnip mosaic virus*, but immunity was lost in the absence of DICER-LIKE proteins DCL4 and DCL2. Systematic analysis of susceptibility and small RNA formation in *Arabidopsis* mutants lacking combinations of RNA-dependent RNA polymerase (RDR) and DCL proteins revealed that the vast majority of virus-derived small interfering RNAs (siRNAs) were dependent on DCL4 and RDR1, although full antiviral defense also required DCL2 and RDR6. Among the DCLs, DCL4 was sufficient for antiviral silencing in inoculated leaves, but DCL2 and DCL4 were both involved in silencing in systemic tissues (inflorescences). Basal levels of antiviral RNA silencing and siRNA biogenesis were detected in mutants lacking RDR1, RDR2, and RDR6, indicating an alternate route to form double-stranded RNA that does not depend on the three previously characterized RDR proteins.

INTRODUCTION

In plants and some animal lineages, such as insects, RNA silencing is a potent defense mechanism against viruses and has remarkable specificity and adaptability (Ding and Voinnet, 2007). To counter this defense mechanism, viruses encode suppressor proteins that interfere with RNA silencing. Antiviral silencing can be conceptualized into initiation, amplification, and systemic spread phases (Voinnet, 2005). Initiation consists of the recognition of the trigger RNA and formation of primary small interfering RNAs (siRNAs), while amplification is characterized by the synthesis of double-stranded RNA (dsRNA) by one or more RNA-dependent RNA polymerases and the formation of secondary siRNA. Systemic spread involves cell-to-cell and phloem-dependent transport of a silencing signal (Ding and Voinnet, 2007).

Dicer-like ribonucleases (DCLs), Argonaute (AGO) proteins, dsRNA binding proteins (DRBs), and RNA-dependent RNA polymerase (RDR) proteins are core components of plant RNA silencing pathways involved in siRNA biogenesis or effector pathways. Four DCLs in *Arabidopsis thaliana* catalyze formation

of microRNAs (miRNAs; DCL1), or 22-nucleotide (DCL2), 24-nucleotide (DCL3), and 21-nucleotide (DCL4) siRNAs from several classes of dsRNA precursors. DCL1 functions with the dsRNA binding protein HYL1 and SERRATE to accurately process predominantly 21-nucleotide miRNAs from foldback precursors (Park et al., 2002; Reinhart et al., 2002; Han et al., 2004; Grigg et al., 2005; Dong et al., 2008). Most, but not all, *Arabidopsis* miRNAs function in association with AGO1 (Vaucheret et al., 2004; Baumberger and Baulcombe, 2005; Qi et al., 2006; Mi et al., 2008). DCL4 functions with DRB4 to process RDR6-dependent dsRNA precursors for trans-acting siRNA (tasiRNA) (Gascioli et al., 2005; Xie et al., 2005; Yoshikawa et al., 2005). Most tasiRNAs also function with AGO1 (Baumberger and Baulcombe, 2005; Mi et al., 2008). DCL3 functions to process RDR2-dependent dsRNA precursors that form at numerous endogenous loci, and at many of these loci, the resulting 24-nucleotide siRNAs function through AGO4/Pol V complexes to direct DRM2-dependent RNA-directed DNA methylation at cytosine positions in a CNN context (Cao and Jacobsen, 2002; Zilberman et al., 2003; Xie et al., 2004; Li et al., 2006; Pontes et al., 2006; Wierzbicki et al., 2009). DCL2 is less well studied than the other DCL proteins, although it is known to play a role in formation of natural antisense siRNA and in transitive silencing of transgene transcripts (Borsani et al., 2005; Bouche et al., 2006; Mlotshwa et al., 2008).

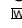
Antiviral RNA silencing depends on some of the core factors that participate in the biogenesis and activity of endogenous siRNAs (Ding and Voinnet, 2007). DCL4 catalyzes formation of 21-nucleotide siRNAs from several RNA and DNA viruses (Blevins et al., 2006; Deleris et al., 2006; Fusaro et al., 2006; Diaz-Pendon et al., 2007). In the absence of DCL4, 22- and

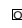
¹ Current address: University of Tokyo, 3-8-1 Komaba, Meguro-ku, Tokyo 153-8902, Japan.

² Current address: Department of Biology, University of California, San Diego, CA 92093.

³ Address correspondence to carrington@cgrb.oregonstate.edu.

The author responsible for distribution of materials integral to the findings presented in this article in accordance with the policy described in the Instructions for Authors (www.plantcell.org) is: James C. Carrington (carrington@cgrb.oregonstate.edu).

 Online version contains Web-only data.

 Open Access articles can be viewed online without a subscription. www.plantcell.org/cgi/doi/10.1105/tpc.109.073056

24-nucleotide-long virus-derived siRNAs are produced by DCL2 and DCL3, respectively (Blevins et al., 2006; Deleris et al., 2006; Fusaro et al., 2006; Diaz-Pendon et al., 2007). DCL1 may play an indirect role as a negative regulator of DCL4 (Qu et al., 2008) and as a facilitator in the biogenesis of geminivirus- and caulimovirus-derived siRNAs (Blevins et al., 2006; Moissiard and Voinnet, 2006). siRNA biogenesis or antiviral silencing have also been shown to be dependent on one or more of RDR1, RDR2, and RDR6 (Mourrain et al., 2000; Qu et al., 2005, 2008; Schwach et al., 2005; Diaz-Pendon et al., 2007; Donaire et al., 2008; Qi et al., 2009; Wang et al., 2010). Systemic RNA silencing in *Arabidopsis* requires RDR1 and RDR6 for amplification of *Cucumber mosaic virus* (CMV)-derived sRNAs (Wang et al., 2010). RDR1 may couple with other defense responses because its expression is induced by salicylic acid (Ji and Ding, 2001; Xie et al., 2001; Yu et al., 2003). It is noted, however, that most studies to date do not clearly link virus-derived siRNA accumulation patterns and bona fide antiviral defense where the virus is actually suppressed or limited. When wild-type viruses are used, the activity of a virus-encoded silencing suppressor can mask the activity of silencing factors. Thus, wild-type plants often exhibit virus susceptibility phenotypes similar to those of mutants that lack RNA silencing factors (Dalmay et al., 2000; Mourrain et al., 2000; Yang et al., 2004; Deleris et al., 2006; Wang et al., 2010).

In this report, a silencing suppressor (HC-Pro)-deficient *Turnip mosaic virus* (TuMV) mutant encoding a green fluorescent protein tag (TuMV-AS9-GFP) was produced and propagated with the aid of a heterologous silencing suppressor provided in trans. The sensitivity of TuMV-AS9-GFP and parental TuMV-GFP viruses to antiviral silencing, and the siRNA-generating patterns, were compared in a series of single and combination *dcl* and *rdr* *Arabidopsis* mutants. The results revealed a distinct set of requirements for antiviral silencing and siRNA generation in inoculated and noninoculated tissues.

RESULTS

Mutational Inactivation of TuMV HC-Pro

Ala-scanning (AS) mutations were introduced in the central domain of *Tobacco etch virus* (TEV) HC-Pro (Kasschau et al., 1997). This resulted in several mutants, including TEV-AS9, which replicated to low levels in tobacco (*Nicotiana tabacum*) protoplasts and were unable to systemically infect plants

(Kasschau et al., 1997). These phenotypes correlated with loss of RNA silencing suppression activity (Kasschau and Carrington, 2001). The AS9 mutation was introduced into the equivalent position in TuMV HC-Pro, and effects on silencing suppression activity were tested using a miRNA-directed silencing assay in which miR171 guides targeting of SCL6-IV transcript (Llave et al., 2002a; Kasschau et al., 2003). Both wild-type and AS9 mutant versions were tested in parallel with several other wild-type and mutant forms of silencing suppressors, including p19 from *Tomato bushy stunt virus* and p21 from *Beet yellows virus* (Chapman et al., 2004). Leaves were agroinfiltrated with constructs to coexpress SCL6-IV mRNA, miR171, and a silencing suppressor. The wild type, but not the mutant, forms of all the suppressors inhibited miR171-guided cleavage of SCL6-IV mRNA (Figure 1), showing that the AS9 mutation debilitated TuMV HC-Pro silencing suppressor activity.

Generation and Propagation of Suppressor-Deficient TuMV-AS9-GFP

We reasoned that infection of *Arabidopsis* plants by a suppressor-deficient TuMV would be arrested at points where antiviral RNA silencing responses are active. This approach would allow analysis of local and systemic infection of *Arabidopsis* plants with inactivating mutations in genes encoding RNA silencing factors. The AS9 mutation was introduced into TuMV-GFP, generating TuMV-AS9-GFP. This mutant accumulated to low levels in *Nicotiana benthamiana*, limiting the potential to propagate the virus to generate reliable inoculum. However, coexpression of constructs expressing the TuMV-AS9-GFP genome with p19 was predicted to rescue the suppressor-defective virus. Infection efficiency of TuMV-AS9-GFP was compared with parental TuMV-GFP in *N. benthamiana*. In fact, p19 rescued TuMV-AS9-GFP, as revealed by fluorescence and TuMV coat protein (CP) accumulation, in a dose-dependent manner (Figure 2A) and enhanced local infection efficiency of TuMV-GFP (Figure 2B). In the absence of p19, the number of TuMV-AS9-GFP infection (multicellular fluorescent) foci was only 36% of that measured for TuMV-GFP. In the presence of p19, infection efficiency of TuMV-AS9-GFP was similar to that of TuMV-GFP (Figure 2B). These results suggest that TuMV-GFP HC-Pro was not able to block completely the silencing response in *N. benthamiana*. Alternatively, or additionally, some viral RNA transcribed from the cDNA cassettes carried by *Agrobacterium tumefaciens* may have been targeted by the silencing machinery before RNA replication was established.

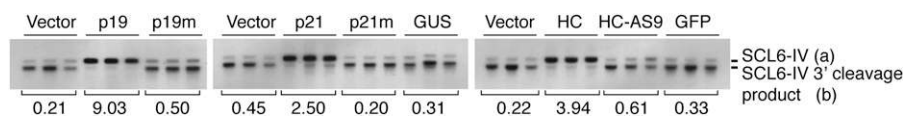


Figure 1. TuMV HC-Pro Containing the AS9 Substitution Lacks RNA Silencing Suppressor Activity in a miR171-Guided Transient Assay in *N. benthamiana* Leaves.

Parental and mutant forms of HC-Pro (HC), or two other suppressors (p19 and p21), were coinfiltrated with 35S:miR171-precursor and 35S:SCL6-IV. Leaves were collected 48 h after infiltration. SCL6-IV mRNA (a) and its miR171-guided 3' cleavage product (b) were analyzed in three independent samples by RNA gel blot assays using randomly primed ^{32}P -radiolabeled probes. For each treatment, the average (a)/(b) ratio for three replicates is indicated. Note that the parental, but not mutant, forms of the suppressors inhibited target cleavage.

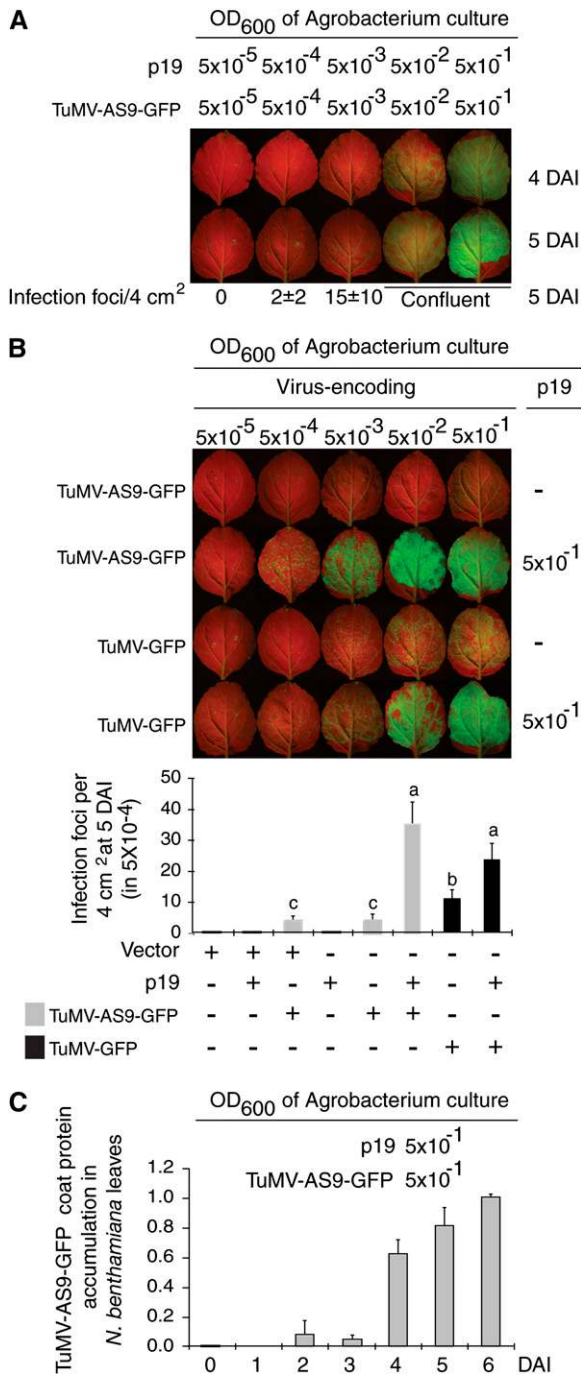


Figure 2. Propagation of TuMV-AS9-GFP in a Transient Infection System.

(A) Infection of *N. benthamiana* leaves by TuMV-AS9-GFP after launching by *Agrobacterium* infiltration in the presence of p19-HA at the indicated cell densities. Infection was measured as the number of multicellular infection foci at 5 DAI under UV light in a 4-cm² area in the middle of the leaf.

(B) Effect of p19-HA on infection efficiency of *N. benthamiana* leaves by TuMV-AS9-GFP and TuMV-GFP. Cultures expressing p19-HA were provided at constant cell density (OD₆₀₀ = 5 × 10⁻¹). Cultures trans-

Systemic infection of *N. benthamiana* by TuMV-GFP was detected at 6 d after inoculation (DAI). By contrast, no systemic infection of *N. benthamiana* by TuMV-AS9-GFP was detected either in the presence or absence of p19 at 15 DAI. At 21 DAI, mild systemic infection of *N. benthamiana* by TuMV-AS9-GFP was detected, although GFP intensity was substantially lower than that observed for TuMV-GFP at 6 DAI.

TuMV-AS9-GFP Is Limited by siRNA-Dependent Antiviral Defense That Is Normally Suppressed by HC-Pro

TuMV-AS9-GFP failed to infect wild-type *Arabidopsis* (Columbia-0 [Col-0]) (Table 1, Figure 3A) despite using enriched, undiluted inoculum (at least 100-fold more concentrated than needed to give 100% systemic infection efficiency in *dcl2-1 dcl3-1 dcl4-2* plants) (see Supplemental Figure 1 online). If immunity of wild-type plants was due entirely or predominantly to effective antiviral silencing in the absence of suppression function, as opposed to the loss of another HC-Pro function, then the mutant should gain infection competence in the siRNA-defective triple mutant with *dcl2-1 dcl3-1 dcl4-2* alleles. For TuMV-GFP, an equal number of local infection foci, and similar amounts of CP, were measured in inoculated leaves and inflorescences of Col-0 and *dcl2-1 dcl3-1 dcl4-2* mutant plants (Figures 3A and 3B). No local infection foci or CP were detected in inoculated leaves or inflorescence, and symptoms did not develop in Col-0 inoculated with TuMV-AS9-GFP (Figures 3A to 3C). By contrast, both local and systemic infection occurred in *dcl2-1 dcl3-1 dcl4-2* mutant plants inoculated with TuMV-AS9-GFP (Figures 3A and 3B). Rescue of the defective infection phenotype in *dcl2-1 dcl3-1 dcl4-2* mutant plants strongly supports the idea that RNA silencing limits the suppressor-defective virus and that HC-Pro promotes systemic infection by suppressing an siRNA-dependent activity. Interestingly, in *dcl2-1 dcl3-1 dcl4-2* triple mutant plants, symptoms caused by TuMV-AS9-GFP were similar to those caused by TuMV-GFP (Figure 3C).

To rigorously confirm that infection of the triple *dcl* mutant by TuMV-AS9-GFP was not due to viral reversion mutations (Garcia-Ruiz and Ahlquist, 2006), a bioassay was done using virus recovered from inflorescences of systemically infected plants at 15 DAI. Virus was concentrated and used to inoculate leaves of Col-0 and *dcl2-1 dcl3-2 dcl4-2* triple mutant plants. While modest numbers of infection foci and systemic infection were detected in the triple mutant, no local or systemic infection

formed with pCB-TuMV-AS9-GFP or pCB-TuMV-GFP were provided at 10-fold dilutions of OD₆₀₀ = 5 × 10⁻¹. Empty vector was used to normalize the cell density to OD₆₀₀ = 1.0. Images were taken at 5 DAI under UV light. Infection foci were plotted for samples receiving cultures at OD = 5 × 10⁻⁴. The histogram shows the average and SE for 16 leaves per treatment.

(C) Time course of accumulation of TuMV-AS9-GFP CP in *N. benthamiana* leaves infiltrated with *Agrobacterium* cultures containing pP19-HA and pCB-TuMV-AS9-GFP (OD₆₀₀ = 5 × 10⁻¹). Relative accumulation was plotted using 6 DAI measurements equal to 1.0. The histogram shows the average and SE for three replicates (individual leaves) per treatment.

Table 1. TuMV-GFP and TuMV-AS9-GFP Infection of Col-0 and Mutant *Arabidopsis*

Genotype	Virus	Plants	Inoculated Rosette	Noninoculated	Bolt	Cauline	Inflorescence	
			Leaves ^a	Rosette	Tissue	Leaves	7 DAI	15 DAI
Col-0	TuMV-AS9-GFP	13	0	0	0	0	0	0
	TuMV-GFP	13	13	13	13	13	13	13
<i>dcl2-1 dcl3-1 dcl4-2</i>	TuMV-AS9-GFP	13	13	13	13	13	10	13
	TuMV-GFP	13	13	13	13	13	11	13

Number of plants showing local and systemic infections were scored by GFP fluorescence under UV illumination. A total of 13 plants were analyzed. Except for a set of inflorescence samples, systemic infection data were from plants at 15 DAI.

^aLocal infection at 7 DAI.

was detected in Col-0 plants (Figure 3D), confirming that the original infections of triple mutant plants by TuMV-AS9-GFP were not due to reversion mutations.

Genome-Wide Profiling of TuMV-Derived siRNAs

Genetic rescue of TuMV-AS9-GFP infection in *dcl2-1 dcl3-1 dcl4-2* mutant plants (Figure 3) shows that TuMV is targeted by an RNA silencing mechanism that requires one or more of the siRNA-generating DCLs. To obtain a detailed view of the siRNAs formed during TuMV infection, deep sequencing analysis of small RNA from Col-0, *dcl2-1 dcl3-1 dcl4-2* triple mutant, and *dcl1-7* single mutant plants was done. The *dcl1-7* mutant, which is a partial loss-of-function mutant, was included because of the possibility that DCL1 might act on foldback structures within the TuMV genome and because of potential effects of DCL1 on the siRNA-generating enzymes (Blevins et al., 2006; Moissiard and Voinnet, 2006; Qu et al., 2008). Wild-type TuMV was used instead of TuMV-GFP to prevent GFP sequences from affecting the formation or accumulation of virus-derived siRNAs. As described for TuMV-GFP (Figure 3B), TuMV accumulated to similar levels in inflorescences of Col-0, *dcl1-7* single, and *dcl2-1 dcl3-1 dcl4-2* triple mutant plants both at 7 and 10 DAI.

Small RNA libraries (three independent biological replicates/treatment) were made from whole plants at both 7 and 10 DAI using sequencing-by-synthesis methods (Fahlgren et al., 2009). The frequency of reads obtained for the internal small RNA standards (Fahlgren et al., 2009) indicated consistent amplicon preparation across libraries. Results described below are from averages of biological replicates.

In infected plants, the number of reads with a perfect match to TuMV varied from 12,000 to 108,000 (Figure 4A; see Supplemental Table 1 online). In Col-0 and *dcl1-7* plants at 7 and 10 DAI, 98% of TuMV-derived small RNAs were 21 to 24 nucleotides long, with the vast majority 21 and 22 nucleotides (Figure 4A). In agreement with a recent study (Donaire et al., 2009), small RNAs originated from both strands, although with a slight bias toward antisense reads (Figure 4A). By contrast, the abundance of virus-derived siRNAs in all size classes was significantly reduced in *dcl2-1 dcl3-2 dcl4-2* triple mutant plants (Figure 4A).

Genome-wide maps of small RNA reads from 10 DAI data sets revealed a high density of TuMV-derived siRNAs along both strands in Col-0 plants. Based on the numbers of reads mapping to the TuMV genome from mock-inoculated plants due to sequencing errors, the false discovery rate in our sequencing was

estimated at 0.0079 per nucleotide and at 0.000053 per read. The distribution trends were similar between Col-0 and *dcl1-7* (Figure 4B), indicating that decreased levels of DCL1 have little effect on the pattern of TuMV-derived small RNA accumulation. By contrast, ~26-fold fewer reads were detected in *dcl2-1 dcl3-1 dcl4-2* triple mutant plants, with the decrease distributed proportionally across the TuMV genome (Figure 4B). As the majority of these reads were 21 and 22 nucleotides in length, it is possible that DCL1 accounted for at least some of the reads in the triple mutant. In all plant genotypes tested, a large number of reads were mapped to the antisense strand of the 5' untranslated region (UTR), specifically to the first 40 nucleotides (Figure 4C; see Supplemental Table 1 online). In *dcl2-1 dcl3-1 dcl4-2* triple mutants, these small RNAs were still prevalent, accounting for 74% of the total TuMV-derived reads (Figure 4C). Similar results were obtained for 21-nucleotide TuMV-derived siRNAs at 7 DAI (see Supplemental Figure 2 online) and for 22-nucleotide siRNAs from both 7 and 10 DAI (see Supplemental Figures 3 and 4 online). However, blot assays showed that the 21-nucleotide siRNA from the 5' UTR region were sensitive to loss of DCL4 (see Supplemental Figure 5 online). In the absence of DCL4, this region yielded siRNAs that were 22 nucleotides in length and dependent on DCL2. The basis for the unusual abundance of antisense 5' UTR-derived siRNAs in each of the sequencing data sets was unclear.

The ratio of antisense-to-sense 21-nucleotide TuMV-derived siRNAs, and the occurrence of each of the four nucleotides at the siRNA 5' position, was analyzed. In Col-0 and *dcl1-7*, the antisense strand bias was modest (see Supplemental Figure 6A online). The antisense/sense strand bias in the *dcl2-1 dcl3-1 dcl4-2* triple mutant was far greater. However, the antisense strand bias was due almost entirely to the relatively high proportion of reads from the antisense 5' UTR region (see Supplemental Figure 6A online). Reads of 21 nucleotides were also grouped by their first nucleotide (A, U, G, or C) and their relative abundance compared with values expected from the nucleotide composition of the sense and antisense strands. The proportion of reads containing a 5' A, C, or G were close to the expected values. TuMV-derived siRNAs with a 5' U, however, were overrepresented in each of Col-0, *dcl1-7*, and the *dcl2-1 dcl3-1 dcl4-2* triple mutant plants, with accumulation levels that were 1.3- to 2.6-fold higher than expected from the TuMV genome nucleotide composition (see Supplemental Figure 6B online). These results suggest that there is preferential accumulation of virus-derived siRNAs with a 5' terminal U, possibly through association with

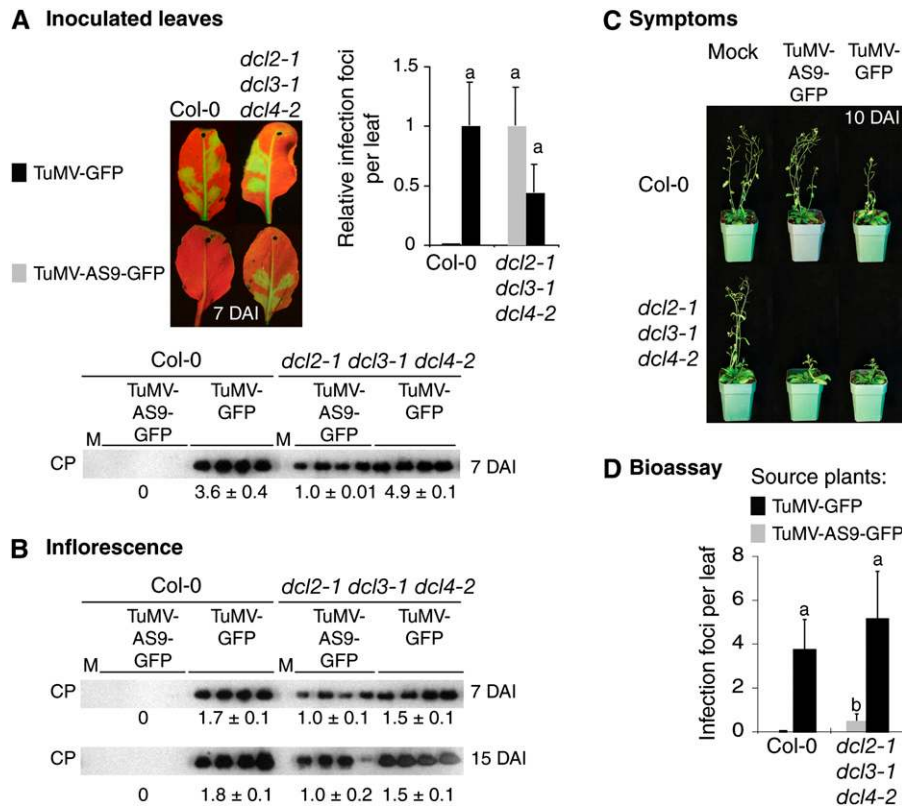


Figure 3. Local and Systemic Infection of *Arabidopsis* by TuMV-GFP and TuMV-AS9-GFP.

(A) Infection efficiency and CP accumulation in inoculated leaves at 7 DAI. Images were taken at 7 DAI under UV light. The number of infection foci for TuMV-GFP and TuMV-AS9-GFP was expressed relative to those in Col-0 (2.6 ± 1.0 foci per leaf) or *dcl2-1 dcl3-1 dcl4-2* (4.6 ± 1.5), respectively. The histogram shows the average and SE for 52 leaves and 13 plants per treatment. For each virus, bars with the same letter are not statistically different (Tukey's test with $\alpha = 0.01$). CP accumulation values (average \pm SE) were normalized to the average number of infection foci. M, mock inoculated.

(B) CP accumulation in inflorescence clusters at 7 and 15 DAI, relative to TuMV-AS9-GFP in *dcl2-1 dcl3-2 dcl4-2* plants. Average and SE for each virus-*Arabidopsis* genotype combination are indicated at the bottom.

(C) Col-0 and *dcl2-1 dcl3-2 dcl4-2* triple mutant plants inoculated with TuMV-AS9-GFP or TuMV-GFP (10 DAI) or mock-inoculated.

(D) Bioassay of TuMV-AS9-GFP from systemically infected *dcl2-1 dcl3-2 dcl4-2* mutant source plants (15 DAI). Average number of infection foci (\pm SE) at 7 DAI were plotted. Bars with the same letter are not statistically different (Tukey's test with $\alpha = 0.01$).

AGO1, which is known to have a 5' U preference (Mi et al., 2008; Montgomery et al., 2008a).

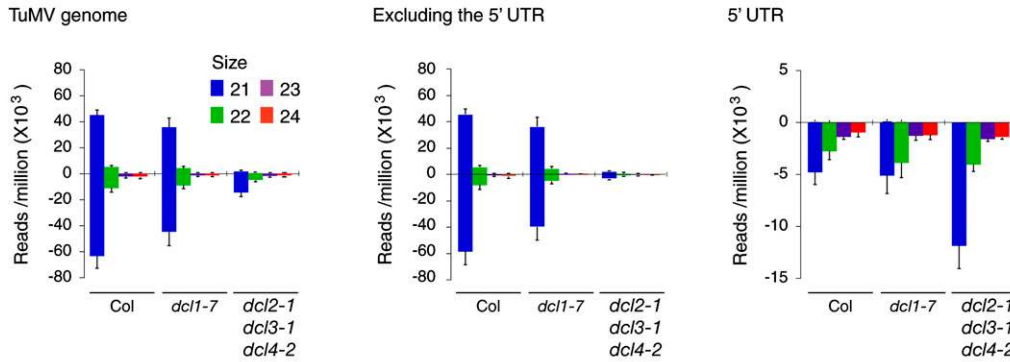
Participation of *Arabidopsis* DCL4 and DCL2 in Antiviral Defense against TuMV

To systematically analyze the requirement of DCL1, DCL2, DCL3, and DCL4 in antiviral RNA silencing and siRNA biogenesis, single and combination mutants were inoculated with parental TuMV-GFP and the suppressor-deficient TuMV-AS9-GFP. TuMV CP (as a reflection of virus accumulation) and virus-derived siRNAs were measured in inoculated rosette leaves, noninoculated cauline leaves, and inflorescence tissues. Virus spread was also monitored using GFP fluorescence in inoculated and noninoculated tissue. The experiment with replicates was repeated twice with similar results.

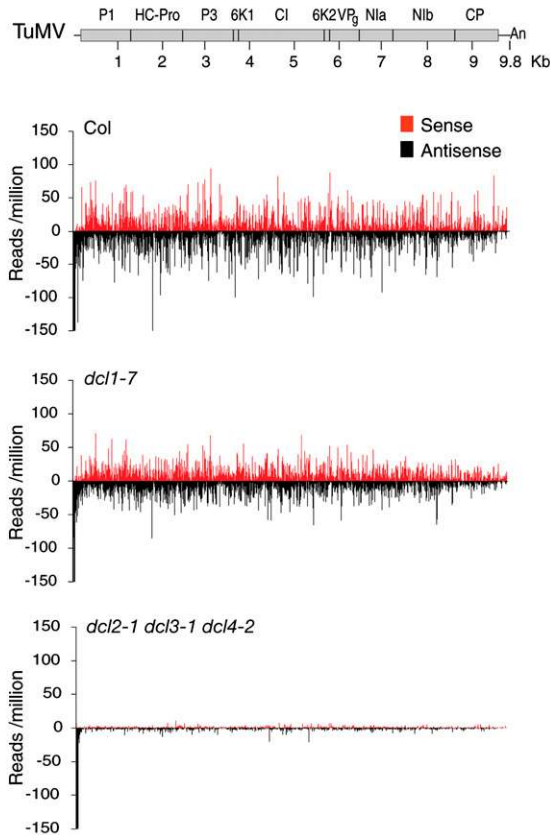
TuMV-GFP infected, both locally and systemically, Col-0 and all *dcl* mutants tested (Table 2, Figure 5A), but no significant

differences ($P > 0.05$) were detected in numbers of TuMV-GFP infection foci in inoculated leaves (Figure 5A) or the general pattern of accumulation in systemic tissues (Table 2, Figures 5B and 5C). By contrast, TuMV-AS9-GFP infection foci in inoculated leaves were visible only in inoculated rosette leaves of mutants containing the *dcl4-2* allele (Table 2, Figure 5A). This was reflected in similar CP levels in inoculated leaves of *dcl4-2* single, *dcl2-1 dcl4-2* double, *dcl3-1 dcl4-2* double, and *dcl2-1 dcl3-1 dcl4-2* triple mutants (Figure 5D; see Supplemental Figure 7 online). Each mutant containing the *dcl4-2* allele also supported systemic infection by TuMV-AS9-GFP to cauline leaves, although combining the *dcl4-2* and *dcl2-1* mutations enhanced virus accumulation by approximately sixfold (Figures 5B and 5D). Interestingly, only mutants containing both *dcl4-2* and *dcl2-1* alleles supported TuMV-AS9-GFP spread to inflorescence tissues (Figure 5D). These data suggest differences between requirements of antiviral defense at the local (DCL4-dependent) and systemic (DCL4- or DCL2-dependent) levels, supporting a

A TuMV-derived siRNA abundance at 10 DAI



B TuMV genome-wide distribution of 21-nt long siRNAs at 10 DAI



C Distribution of 21-nt long siRNAs in the 5' UTR at 10 DAI

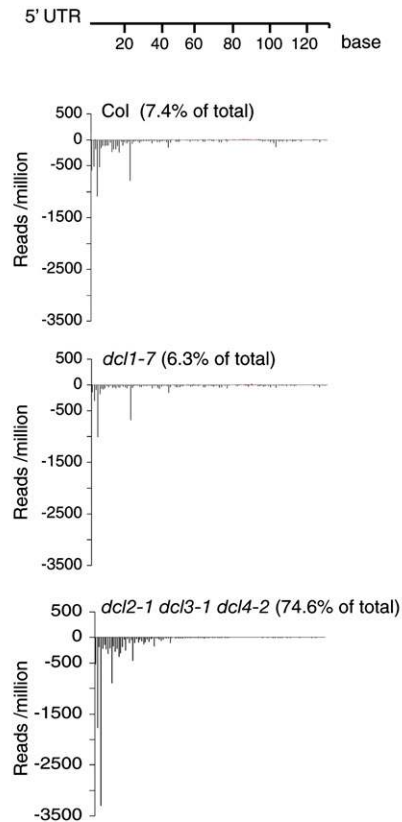


Figure 4. Profile of TuMV-Derived siRNAs in Whole *Arabidopsis* Plants at 10 DAI.

Values are averages and SE from three replicate libraries, normalized to reads/million. Sense and antisense polarity reads were plotted on the y axis in the positive and negative directions, respectively.

(A) Abundance, by size class and polarity, of TuMV-derived small RNAs at 10 DAI in three plant genotypes.

(B) Genome-wide distribution of 21-nucleotide TuMV-derived siRNAs at 10 DAI. The scale was capped at 150 reads.

(C) Distribution of 21-nucleotide siRNAs mapping to the 5' UTR region of TuMV RNA at 10 DAI. Numbers in parenthesis indicate the percentage of antisense TuMV-derived reads that mapped to the 5' UTR. Based on length, a random distribution of siRNA along the TuMV genome would yield 1.3% mapping to the 5' UTR.

Table 2. TuMV-GFP and TuMV-AS9-GFP Infection in Single and Multiple *dcl* *Arabidopsis* Mutants

Virus	<i>Arabidopsis</i> Genotype	Plants	Inoculated Rosette Leaves ^a	Noninoculated Rosette	Bolt Tissue	Cauline Leaves	Inflorescences		
							7 DAI	15 DAI	% ^b
TuMV-GFP									
	Col-0	14	14	14	14	14	11	14	100
	<i>dcl1-7</i>	14	14	14	14	14	0	14	100
	<i>dcl2-1</i>	14	14	14	14	14	10	14	100
	<i>dcl3-1</i>	14	14	14	14	14	8	14	100
	<i>dcl4-2</i>	14	14	14	14	14	6	14	100
	<i>dcl2-1 dcl3-1</i>	14	14	14	14	14	9	14	100
	<i>dcl2-1 dcl4-2</i>	14	14	14	14	14	6	14	100
	<i>dcl3-1 dcl4-1</i>	14	14	14	14	14	7	14	100
	<i>dcl2-1 dcl3-1 dcl4-2</i>	14	14	14	14	14	7	14	100
TuMV-AS9-GFP									
	Col-0	14	0	0	0	0	0	0	0
	<i>dcl1-7</i>	14	0	0	0	0	0	0	0
	<i>dcl2-1</i>	14	0	0	0	0	0	0	0
	<i>dcl3-1</i>	14	0	0	0	0	0	0	0
	<i>dcl4-2</i>	14	14	14	14	14	0	0	0
	<i>dcl2-1 dcl3-1</i>	14	0	0	0	0	0	0	0
	<i>dcl2-1 dcl4-2</i>	14	14	14	14	14	8	14	100
	<i>dcl3-1 dcl4-1</i>	14	14	14	14	14	0	0	0
	<i>dcl2-1 dcl3-1 dcl4-2</i>	14	14	14	14	14	8	14	100

Number of plants showing local and systemic infection were scored by GFP fluorescence under UV illumination. A total of 14 plants were analyzed. Except for a set of inflorescence samples, systemic infection data were from plants at 15 DAI.

^aLocal infection at 7 DAI.

^bPercentage (average of 14 plants) of inflorescence clusters showing GFP at 15 DAI.

model for cooperative interaction or redundancy between DCL4 and DCL2 during systemic antiviral silencing.

Consistent with previous findings (Xie et al., 2004; Fusaro et al., 2006) and with our sequencing results (Figure 4A), TuMV-GFP-derived siRNAs in Col-0 plants were predominantly 21 nucleotides in all tissues tested (Figures 6A to 6C). As was most evident in cauline leaves and inflorescences, the loss of DCL4 resulted in a size shift of the siRNA population to 22 nucleotides (Figures 6B to 6D). Loss of both DCL2 and DCL4 led to accumulation of 24-nucleotide, DCL3-dependent siRNAs (Figures 6B and 6C). All size classes of siRNA were lost in the *dcl2-1 dcl3-1 dcl4-2* triple mutant (Figures 6A to 6C). Thus, although there was a clear dependence on DCL4 for the abundant 21-nucleotide TuMV siRNA, and DCL2 and DCL3 could recognize TuMV-derived dsRNA to make 22- and 24-nucleotide siRNA, respectively, there was no correlation between any measurable siRNA accumulation patterns and antiviral defense against the suppressor-competent TuMV-GFP.

TuMV-AS9-GFP-derived siRNAs in inoculated leaves were below detection levels in all plants (Figure 6A), although they were detected at low levels in cauline or inflorescence tissues of most mutant plants in which systemic spread was detected (Figures 6A to 6C and 6E). As systemic infection by TuMV-AS9-GFP required loss of DCL4 and (in inflorescences) DCL2, the sizes of virus-derived siRNAs reflected the availability of DCLs. In cauline leaves of *dcl4-2* single or *dcl3-1 dcl4-2* double mutants, TuMV-AS9-GFP-derived siRNAs were 22 nucleotides in length and dependent on DCL2; in inflorescence tissues of *dcl2-1 dcl4-2* double mutant plants, the DCL3-dependent 24-nucleotide

size class of siRNA was detected (Figures 6B, 6C, and 6E). All TuMV-AS9-GFP siRNAs were lost in the triple mutant.

Participation of *Arabidopsis* RDR1, RDR2, and RDR6 in Antiviral Defense against TuMV

In *Arabidopsis* and *N. benthamiana*, biogenesis of virus-derived siRNAs has been shown to involve RDR genes (Diaz-Pendon et al., 2007; Donaire et al., 2008; Qu et al., 2008; Wang et al., 2010), but virus accumulation was not always enhanced in *rdr* mutants (Diaz-Pendon et al., 2007; Donaire et al., 2008; Qi et al., 2009). *Arabidopsis* RDR1 participates in the biogenesis of CMV- and Tobacco mosaic virus-derived siRNAs (Diaz-Pendon et al., 2007; Qi et al., 2009; Wang et al., 2010), while the biogenesis of Tobacco rattle virus (TRV)-derived siRNAs involves the combined activity of RDR1, RDR2, and RDR6 (Donaire et al., 2008). Loss of RDR6 enhances accumulation of CMV (Mourrain et al., 2000; Wang et al., 2010). As with the *dcl* mutant series, a systematic analysis of the roles of RDR1, RDR2, and RDR6 in anti-TuMV silencing and siRNA biogenesis was explored using both suppressor-competent and suppressor-defective viruses. Each experiment was repeated four times with similar results.

TuMV-GFP systemically infected Col-0 and all *rdr* mutants tested. In all single and combination *rdr* mutants, TuMV-GFP infection induced symptoms similar to the observed for Col-0 (Figures 3C and 7C), and no significant differences ($P > 0.05$) were detected in numbers of infection foci in inoculated leaves or virus accumulation in cauline leaves or inflorescence tissues (Table 3, Figures 7A to 7E; see Supplemental Figure 8 online).

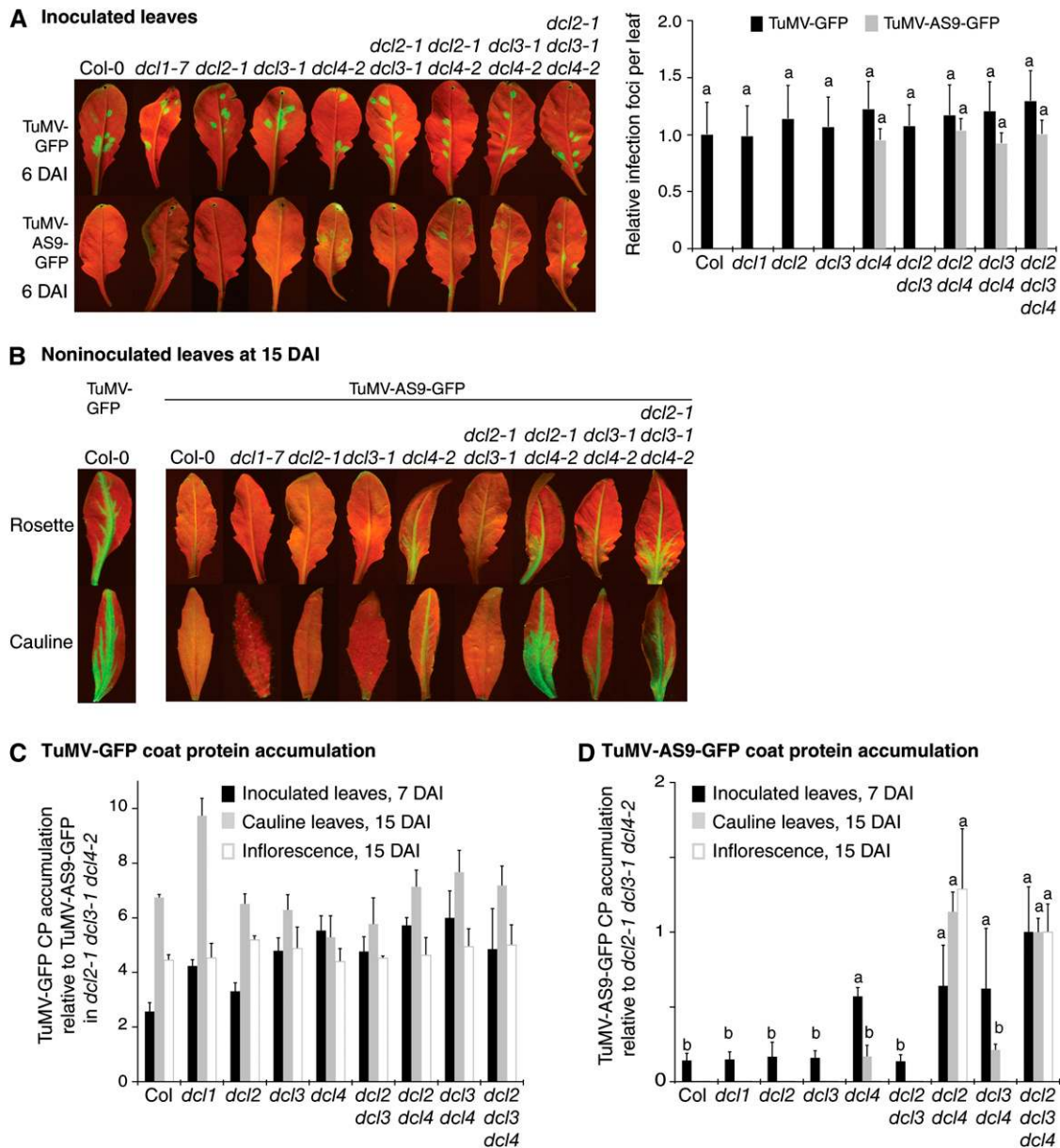


Figure 5. Local and Systemic Infection of *Arabidopsis* *dcl* Mutants by TuMV-GFP and TuMV-AS9-GFP.

(A) Local infection foci in inoculated rosette leaves at 6 DAI. The histogram shows average (+ SE) number of foci from 14 plants, each with four inoculated leaves. For each virus, bars with the same letter are not statistically different (Tukey's test with $\alpha = 0.01$). TuMV-GFP and TuMV-AS9-GFP infection efficiency is expressed relative to Col-0 and to *dcl2-1 dcl3-2 dcl4-2*, respectively.

(B) GFP fluorescence in noninoculated rosette and cauline leaves from plants inoculated with TuMV-AS9-GFP at 15 DAI. TuMV-GFP infection of Col-0 is shown for comparison.

(C) TuMV-GFP accumulation (CP, average + SE) in leaves (7 and 15 DAI) and inflorescence (15 DAI), expressed relative to accumulation of TuMV-AS9-GFP CP in *dcl2-1 dcl3-2 dcl4-2*.

(D) TuMV-AS9-GFP accumulation (CP, average + SE) in leaves (7 and 15 DAI) and inflorescence (15 DAI), relative to *dcl2-1 dcl3-2 dcl4-2*. Within each tissue, bars with the same letter are not statistically different (Tukey's test with $\alpha = 0.01$).

However, there were significant ($P < 0.05$) differences in TuMV-GFP-derived siRNA accumulation among the mutants. TuMV-GFP siRNAs in *rdr2-1* and *rdr6-15* single, and in *rdr2-1 rdr6-15* double, mutants accumulated to similar levels as those in Col-0 (Figures 8A to 8D). By contrast, accumulation of siRNAs derived

from the cylindrical inclusion (CI) or from the 5' UTR (see Supplemental Figure 5B online) of TuMV was significantly reduced in each single, double, and triple mutants harboring the *rdr1-1* allele (Figures 8A to 8D), indicating that RDR1 is a major contributor to biogenesis of TuMV-derived siRNAs. However, in

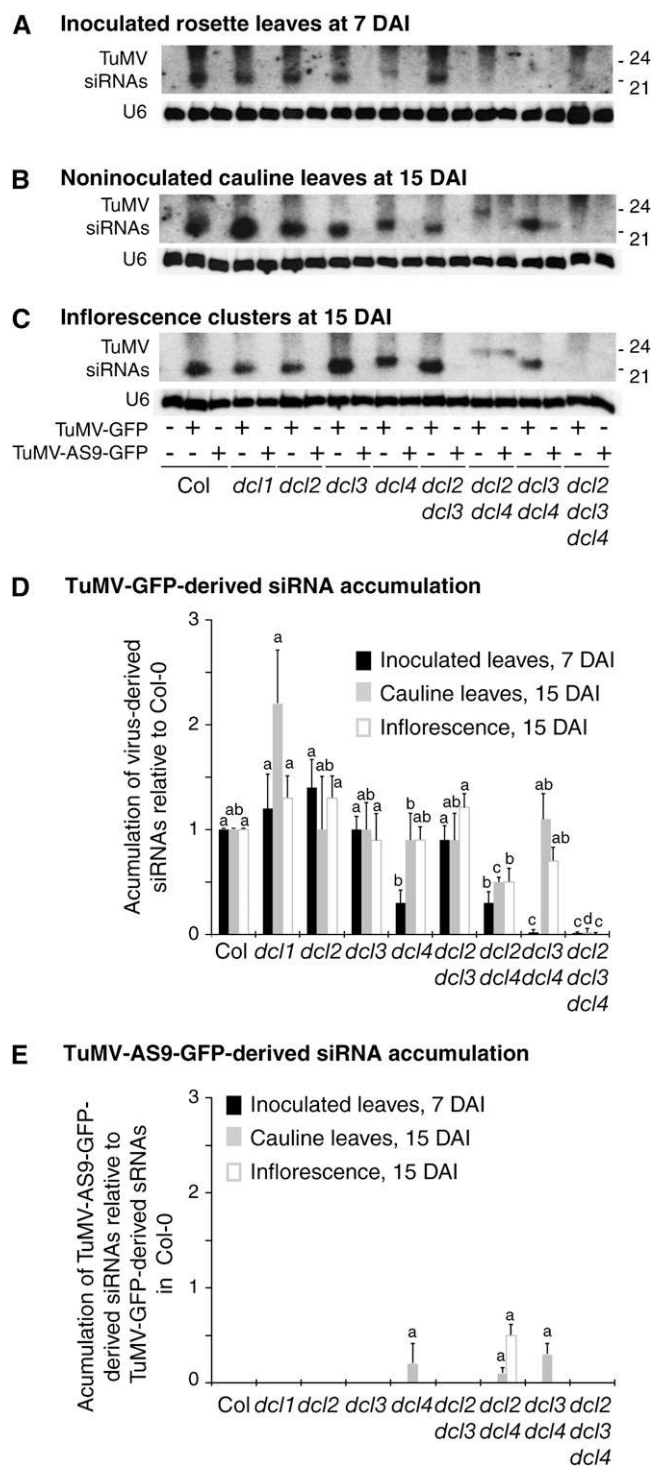


Figure 6. Accumulation of TuMV-GFP- and TuMV-AS9-GFP-Derived siRNAs in *Arabidopsis dcl* Mutants.

Virus-derived siRNA were detected using ^{32}P -radiolabeled probes made by random priming of cDNA corresponding to the CI protein coding region. Virus-derived siRNA signals were normalized to U6 RNA signals from the same blots. In *dcl4-2* single and *dcl3-1 dcl4-2* double mutants, siRNAs were 22 nucleotides long. In *dcl2-1 dcl4-2* double mutants, siRNAs were 24 nucleotides long.

each tissue, a basal level of TuMV-GFP-derived siRNAs was detected in the *rdr1-1 rdr2-1 rdr6-15* triple mutant (Figures 8A to 8D). These levels were higher than those detected in the siRNA-defective *dcl2-1 dcl3-2 dcl4-2* triple mutant, suggesting an alternative source of dsRNA during infection. In all *rdr* mutants, siRNAs were 21 nucleotides in length, which was consistent with dsRNA processing primarily by DCL4 (Figure 3A). Surprisingly, all single, double, and triple *rdr* mutants inoculated with suppressor-defective TuMV-AS9-GFP yielded a similar number of infection foci, whereas no foci were detected in Col-0 plants (Figure 7A, Table 3). Infection foci were less bright and CP accumulated to lower levels in inoculated leaves of each *rdr* single or combination mutant compared with what was detected in *dcl2-1 dcl3-2 dcl4-2* plants (Figures 7A and 7E).

While TuMV-AS9-GFP was restricted to initial infection foci in *rdr2-1* plants, the virus was able to move to cauline leaves and inflorescence tissue in each single or combination mutant containing either *rdr1-1* or *rdr6-15* alleles (Table 3, Figures 7B and 7E). Thus, RDR1 and RDR6 act additively or cooperatively to limit systemic infection of the suppressor-defective virus. However, in the *rdr* triple mutant, TuMV-AS9-GFP failed to induce symptoms (Figure 7C) and accumulated to lower levels than in the *dcl* triple mutant (Figure 7E; see Supplemental Figure 8 online), supporting the idea of a basal level of antiviral silencing that is RDR1, RDR2, and RDR6 independent. In fact, a low level of TuMV-AS9-GFP-derived siRNAs was detected in the both the *rdr1-1 rdr6-15* double and *rdr1-1 rdr2-1 rdr6-15* triple mutants (Figures 8B and 8C).

DISCUSSION

Extensive use was made of TuMV-GFP and suppressor-deficient TuMV-AS9-GFP to expose antiviral silencing activities in *Arabidopsis*. Wild-type plants were immune to TuMV-AS9-GFP, but immunity was effectively suppressed by loss of DCL2 and DCL4, indicating that TuMV normally masks the effects of an siRNA-dependent antiviral response. As noted previously (Deleris et al., 2006; Diaz-Pendon et al., 2007; Qu et al., 2008), suppressor-mediated masking has hampered interpretation of genetic analyses to understand antiviral silencing. This reinforces the requirement to examine suppressor-deficient viruses to gauge the contributions of silencing components during antiviral RNA silencing.

siRNA Biogenesis and Antiviral Silencing

Abundance of TuMV-derived siRNA within infected plants is a rather inaccurate reflection of antiviral silencing activity. During TuMV-GFP infection, large pools of 21-nucleotide siRNA

(A) Inoculated rosette leaves at 7 DAI.

(B) Noninoculated cauline leaves at 15 DAI.

(C) Inflorescence clusters at 15 DAI.

(D) Average (+ SE) TuMV-GFP-derived siRNA signal intensity in four independent replicates in each genotype. Within each tissue, bars with the same letter are not statistically different (Tukey's test with $\alpha = 0.01$).

(E) Accumulation of TuMV-AS9-GFP-derived siRNAs.

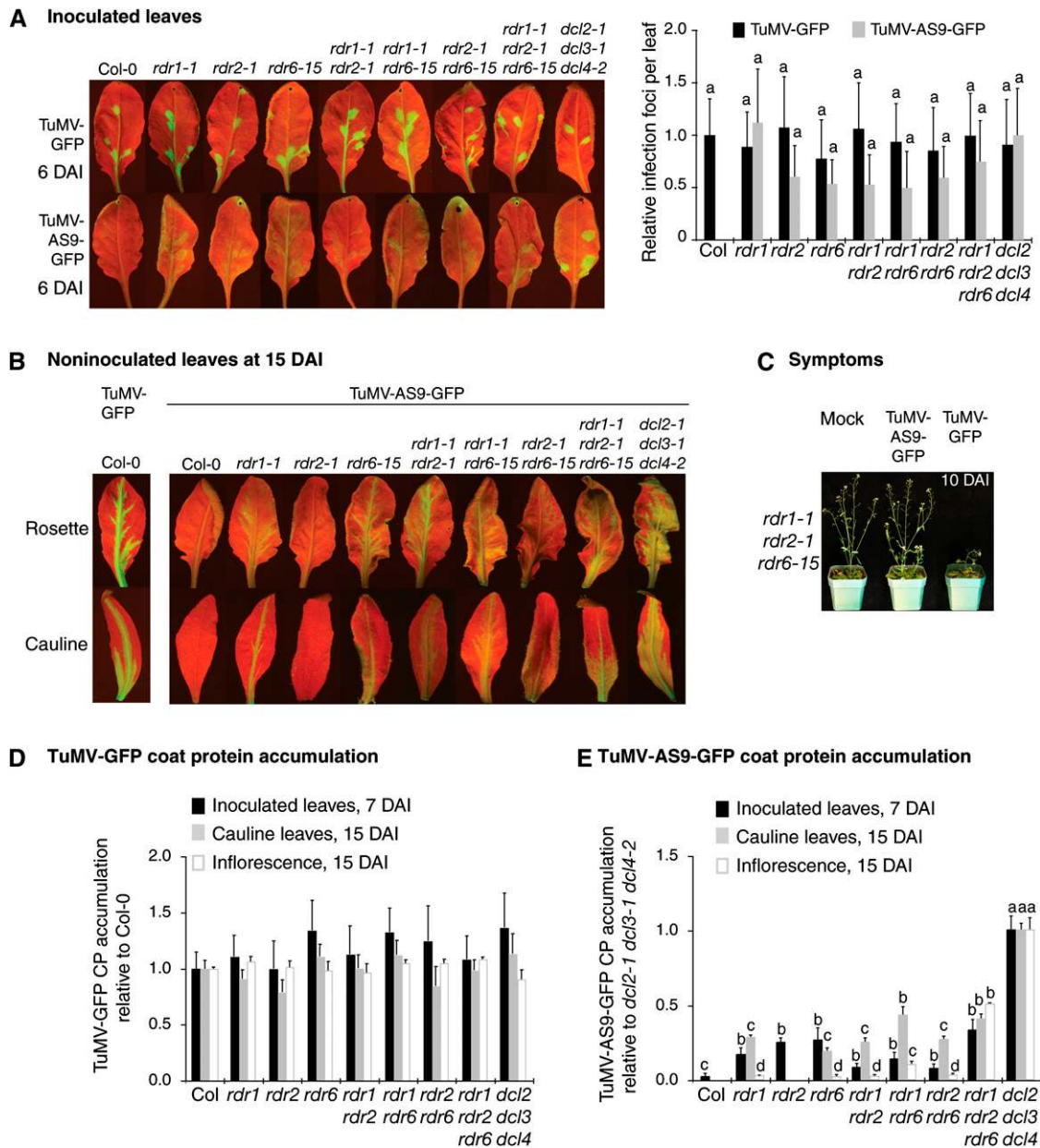


Figure 7. Local and Systemic Infection *Arabidopsis* *rdr* Mutants by TuMV-GFP and TuMV-AS9-GFP.

(A) Local infection foci in inoculated rosette leaves at 6 DAI. The histogram shows average (+ SE) number of foci from 14 plants, each with four inoculated leaves. For each virus, bars with the same letter are not statistically different (Tukey's test with $\alpha = 0.01$). TuMV-GFP and TuMV-AS9-GFP infection efficiency is expressed relative to Col-0 and to *dcl2-1 dcl3-2 dcl4-2*, respectively.

(B) GFP fluorescence in noninoculated rosette and cauline leaves from plants inoculated with TuMV-AS9-GFP, at 15 DAI. TuMV-GFP infection of Col-0 is shown for comparison.

(C) *rdr1-1 rdr2-1 rdr6-15* triple mutant plants (10 DAI) inoculated with TuMV-AS9-GFP, TuMV-GFP, or mock inoculated.

(D) TuMV-GFP accumulation (CP, average + SE) in leaves (7 and 15 DAI) and inflorescence (15 DAI), relative to CP levels in Col-0. Within each tissue type, no statistically significant differences (Tukey's test with $\alpha = 0.01$) were detected between genotypes.

(E) TuMV-AS9-GFP CP accumulation in leaves (7 and 15 DAI) and inflorescence (15 DAI), relative to *dcl2-1 dcl3-2 dcl4-2*. Within each tissue, bars with the same letter are not statistically different (Tukey's test with $\alpha = 0.01$).

Table 3. TuMV-GFP and TuMV-AS9-GFP Infection in Single and Multiple *rdr* *Arabidopsis* Mutants

Virus	<i>Arabidopsis</i> Genotype	Plants	Inoculated Rosette	Noninoculated	Bolt	Cauline	Inflorescences		
			Leaves ^a	Rosette	Tissue	Leaves	7 DAI	15 DAI	% ^b
TuMV-GFP									
	Col-0	14	14	14	14	14	14	14	100
	<i>rdr1-1</i>	14	14	14	14	14	14	14	100
	<i>rdr2-1</i>	14	14	14	14	14	14	14	100
	<i>rdr6-15</i>	14	14	14	14	14	14	14	100
	<i>rdr1-1 rdr2-1</i>	14	14	14	14	14	14	14	100
	<i>rdr1-1 rdr6-15</i>	14	14	14	14	14	14	14	100
	<i>rdr2-1 rdr6-15</i>	14	14	14	14	14	14	14	100
	<i>rdr1-1 rdr2-1 rdr6-15</i>	14	14	14	14	14	14	14	100
	<i>dcl2-1 dcl3-1 dcl4-2</i>	14	14	14	14	14	13	14	100
TuMV-AS9-GFP									
	Col-0	14	0	0	0	0	0	0	0
	<i>rdr1-1</i>	14	14	14	14	14	0	2	0.45
	<i>rdr2-1</i>	14	14	0	0	0	0	0	0
	<i>rdr6-15</i>	14	14	14	14	14	0	0	0
	<i>rdr1-1 rdr2-1</i>	14	14	14	14	14	0	0	0
	<i>rdr1-1 rdr6-15</i>	14	14	14	14	14	12	14	51
	<i>rdr2-1 rdr6-15</i>	14	14	14	14	14	0	0	0
	<i>rdr1-1 rdr2-1 rdr6-15</i>	14	14	14	14	14	9	14	49
	<i>dcl2-1 dcl3-1 dcl4-2</i>	14	14	14	14	14	14	14	100

Number of plants showing local and systemic infection were scored by GFP fluorescence under UV illumination. A total of 14 plants were analyzed. Except for a set of inflorescence samples, systemic infection data were from plants at 15 DAI.

^aLocal infection at 7 DAI.

^bPercentage (average of 14 plants) of inflorescence clusters showing GFP at 15 DAI.

accumulated concomitant with amplification and spread of the virus in wild-type plants (Figure 4B). This can be reconciled with the known activity of HC-Pro in sequestration or inactivation of small RNAs, whereby siRNAs accumulate but lack activity (Lakatos et al., 2006). More importantly, this effect points out the need to carefully analyze both siRNA-related activities and antiviral immunity.

DCL4 and RDR1 were revealed as major contributors to the abundant pool of 21-nucleotide TuMV-GFP-derived siRNAs (Figures 6D and 8D). However, in the absence of DCL4, 22-nucleotide DCL2-dependent siRNAs were formed. Furthermore, in the absence of DCL4 and DCL2, 24-nucleotide DCL3-dependent siRNAs were produced (Figure 6D). However, the 24-nucleotide siRNA (in the *dcl2-1 dcl4-2* double mutant) had no apparent effect on antiviral silencing, and the 22-nucleotide siRNA (in the *dcl4-2* mutant) did not restrict movement of the suppressor-defective virus to cauline leaves. Thus, while each of the siRNA-generating DCL proteins has hierarchical access to double-stranded viral RNA, it is clear that different size classes of siRNA function differentially, or not at all (24-nucleotide siRNAs), during antiviral defense. Similar conclusions were reached previously for infection of *Arabidopsis* by TRV (Deleris et al., 2006).

RDR6 is an important component of anti-TuMV silencing, as RDR6 was essential (along with RDR1) for restricting systemic infection by the suppressor-defective virus (Figure 7E). However, the *rdr6-15* mutation had no detectable effect on the biogenesis of TuMV-GFP-derived siRNAs (Figure 8). Thus, either RDR6 contributes very little to the dsRNA pool from which most siRNAs arise, or RDR6 activity is inhibited by HC-Pro during infection by TuMV-GFP.

Modular Activity of RNA Silencing Factors in Antiviral Silencing

The DCL4-dependent virus-derived siRNAs were necessary and sufficient (among the DCL family) to prevent initial infection foci in TuMV-AS9-GFP-inoculated leaves (Figures 5 and 6). By contrast, DCL2-dependent siRNAs were neither necessary nor sufficient to limit infections of TuMV-AS9-GFP in either inoculated leaves or cauline leaves. Interestingly, DCL2 limited systemic infection of inflorescence tissues in the absence of DCL4 (Figure 5D, Table 2). Why, in the absence of DCL4, is DCL2 sufficient to prevent viral infection in inflorescences but not in inoculated leaves? It is likely not due to differential expression, as both of DCL4 and DCL2 are expressed at similar levels in both leaf and inflorescence tissues (Schmid et al., 2005). These results also cannot be explained by differential access by DCL2 to dsRNA substrates because 22-nucleotide-long TuMV-GFP-derived siRNAs were detected both in leaves and in inflorescence of *dcl4-2* single mutant plants (Figure 6D). A quantitative DCL2-mediated reduction of local viral accumulation resulting in limited systemic spread is also unlikely, as DCL2 alone had no effect on suppressor-deficient virus accumulation in inoculated leaves (Figures 5A and 5D). Several nonmutually exclusive scenarios might explain the differential role of DCL2 in siRNA biogenesis and antiviral defense in inoculated leaves and inflorescences. DCL2 may have unique functions or cofactors in inflorescences or yield siRNAs that function with inflorescence-specific AGO effectors. Alternatively, in inoculated leaves, DCL2 might participate in the formation of a mobile, non-cell-autonomous signal that potentiates an antiviral response in

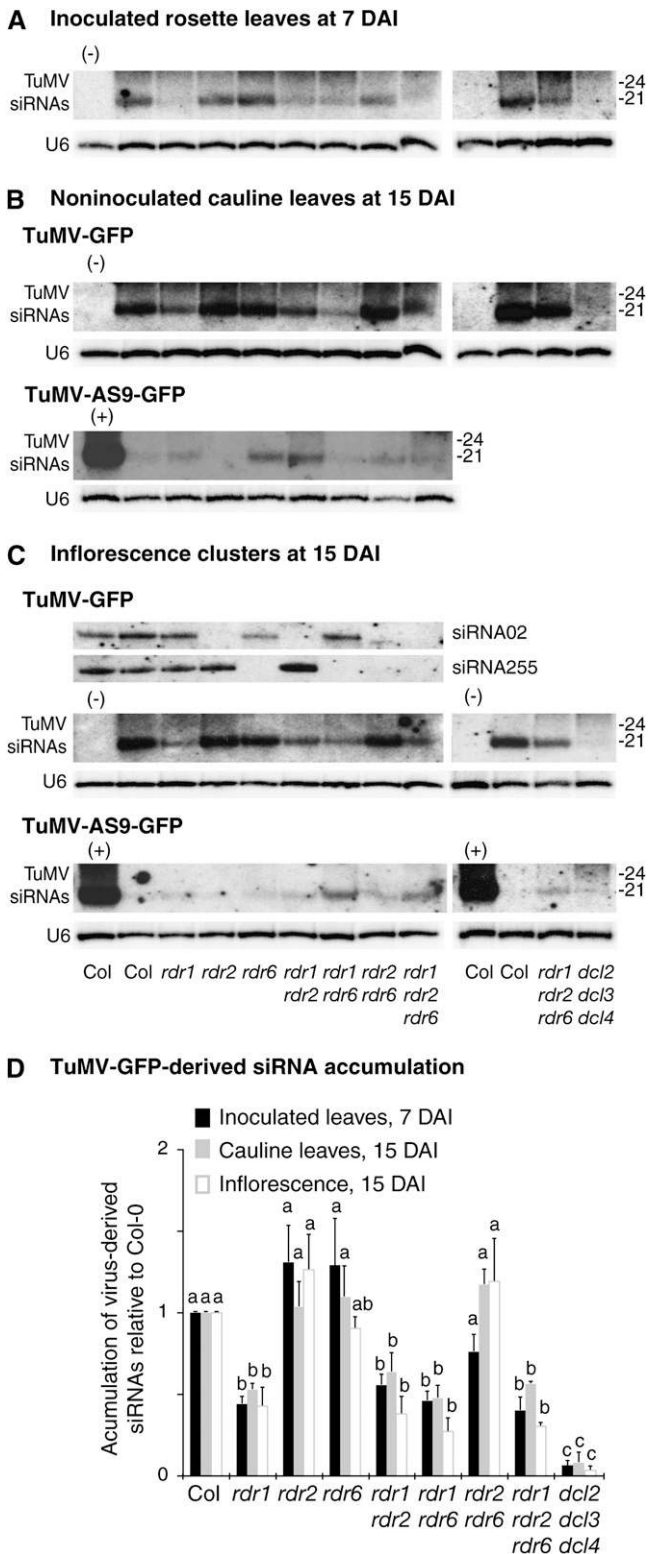


Figure 8. Accumulation of TuMV-GFP- and TuMV-AS9-GFP-Derived siRNAs in *Arabidopsis* *rdr* Mutants.

Blot assays were done as described in Figure 6.

(A) Inoculated leaves at 7 DAI.

inflorescences. Interestingly, DCL2 was shown to function during transitive amplification of transgene silencing in an RDR6-dependent manner (Mlotshwa et al., 2008).

No detectable effect was associated to RDR2 or RDR6 on accumulation of TuMV-GFP-derived siRNAs (Figures 7 and 8). However, the appearance of infection foci in inoculated leaves of *rdr1-1*, *rdr2-1*, and *rdr6-15* single mutant plants means that the three RDR proteins work coordinately to limit primary infections. Thus, RDR1, RDR2, and RDR6 are complementary, or act in coordination, to restrict infection in primarily inoculated leaves by an unknown mechanism. Both RDR1 and RDR6 were necessary, but individually insufficient, to prevent systemic infection of cauline leaves. In inflorescence tissues, RDR1 and RDR6 were redundant in restricting infection, as TuMV-AS9-GFP was largely restricted from inflorescence tissues in single *rdr1-1* and *rdr6-15* mutants (Figure 7E, Table 3).

One hypothesis to explain the differential effects associated to RDR1 and RDR6 in the biogenesis of virus-derived siRNAs and in antiviral RNA silencing is that *Arabidopsis* RDR-dependent pathways differ in their sensitivity to HC-Pro-mediated silencing suppression. RDR1 and RDR6 are known to have distinct functions or properties. RDR6, but not RDR1, participates in the biogenesis of tasiRNA (Peragine et al., 2004; Vazquez et al., 2004) and in posttranscriptional trans-gene silencing (Dalmay et al., 2000; Mourrain et al., 2000). Furthermore, RDR1, but not RDR6, is induced by salicylic acid or pathogen infection (Xie et al., 2001). Differential sensitivity to HC-Pro might constitute an additional difference. Alternatively, triggers that activate RDR1- and RDR6-dependent activities might be differentially sensitive to HC-Pro. As proposed for RDR6-dependent formation of dsRNA during tasiRNA formation, it is postulated that RDR-dependent amplification during virus infection would occur after initial AGO-siRNA targeting events on TuMV genomic RNA (Montgomery et al., 2008a, 2008b). The initial AGO-siRNA targeting events might involve cleavage and deadenylation of viral RNA as well as noncleavage association of AGO-siRNA complexes with viral RNA. The associated AGO protein might serve as a flag for direct or indirect recruitment of RDR1 and RDR6. This line of reasoning implies that RDR1 and RDR6 triggers are different.

Entry of Viral RNA into Silencing Pathways

Two lines of evidence support the existence of an antiviral dsRNA-generating mechanism that is both independent from RDR1, RDR2, and RDR6 and that is insensitive to HC-Pro. First, suppressor-deficient TuMV-AS9-GFP accumulated to lower levels in *rdr1-1 rdr2-1 rdr6-15* than in *dcl2-1 dcl3-2 dcl4-2* triple

(B) Noninoculated cauline leaves at 15 DAI.

(C) Inflorescence clusters at 15 DAI. Both TuMV-GFP and TuMV-AS9-GFP-inoculated samples were tested.

(D) Average (+ SE) TuMV-GFP-derived siRNA signal intensity in four independent replicates in each genotype. Within each tissue, bars with the same letter are not statistically different (Tukey's test with $\alpha = 0.01$). (-) and (+) indicate Col-0 mock-inoculated or TuMV-GFP infected, respectively.

mutants (Figure 7E), indicating an alternate source of dsRNA that functions as a substrate for DCL activity in the triple *rd* mutant. Second, low but consistent levels of virus-derived siRNAs were detected in *rd1-1 rd2-1 rd6-15* triple mutant plants infected with TuMV-GFP (Figure 8), which is consistent with similar findings by Donaire et al. (2008). The presumed dsRNA in *rd1-1 rd2-1 rd6-15* triple mutants could arise from the activities of one or more of RDR3, RDR4, and/or RDR5, none of which have been shown to be functional. Alternatively, in *rd1-1 rd2-1 rd6-15* triple mutants, the siRNA may be the result of processing of dsRNA from viral RNA replication products or intermediates as described for *Flock house virus* infections of *Drosophila melanogaster* (Aliyari et al., 2008; Flynt et al., 2009).

The initial trigger events for recognition of TuMV RNA remain unclear. Analysis of *Cymbidium ringspot tumbovirus*-derived siRNAs in *N. benthamiana* showed that sense siRNA predominated over antisense siRNAs and that segments of the genome with extensive secondary structure yielded siRNAs at higher frequency (Molnar et al., 2005). Rather than a sense strand bias, a slight antisense bias was detected in most of the TuMV siRNA libraries analyzed (Figure 4A; see Supplemental Figure 6 online), although this could be reflective of modest stabilization differences due to the likelihood of siRNAs forming with 5' ends containing each of the four possible nucleotides. Given that the antisense strand has a higher proportion of uracil than does the sense strand, it would be expected that more siRNA would have a 5' U residues, which would promote association with, and stabilization by, AGO1 (Mi et al., 2008; Montgomery et al., 2008a). Although no miRNA precursor-like structures were found in TuMV using criteria established for canonical miRNA precursors (Meyers et al., 2008), it is still possible that initial trigger events involve DCL-mediated cleavage of positive-strand viral RNA. These putative events could even be catalyzed by DCL1, even though the small RNA profile in *dcl1-7* mutant plants was similar to that from wild-type plants. The *dcl1-7* allele is a partial loss-of-function allele, meaning that residual activity might yield sufficient numbers of primary processing events that initiate amplification cycles that involve RDR1 and RDR6.

METHODS

Plant Materials

Nicotiana benthamiana plants used for virus propagation or transient RNA silencing assays were 40 d old and had six to eight leaves at the time of inoculation or infiltration. *Arabidopsis thaliana* mutant lines *rd1-1*, *rd2-1*, *rd6-15*, *dcl1-7*, *dcl2-1*, *dcl3-1*, *dcl4-2*, *dcl2-1 dcl3-1*, *dcl2-1 dcl4-2*, *dcl3-1 dcl4-2*, and *dcl2-1 dcl3-1 dcl4-2* were described (Allen et al., 2004, 2005; Xie et al., 2004, 2005; Deleris et al., 2006). *rd1-1 rd2-1*, *rd1-1 rd6-15*, *rd2-1 rd6-15*, and *rd1-1 rd2-1 rd6-15* were generated by standard crossing. While *dcl1-7* is a partial loss of function allele (Xie et al., 2004), all other lines carry null alleles. Plants were maintained in a greenhouse or a growth room at 22°C with a 16-h-light/8-h-dark cycle. Thirty-day-old *Arabidopsis* plants were inoculated.

DNA Plasmids and Constructs

Recombinant plasmids and constructs used are described in the Supplemental Methods online.

Transient RNA Silencing Assays in *N. benthamiana*

Agrobacterium tumefaciens infiltration of *N. benthamiana* was done as described (Johansen and Carrington, 2001). *A. tumefaciens* GV3101 contained 35S:miR171, 35S:SCL6-IV (Llave et al., 2002b), 35S:GFP, 35S:GUS (Johansen and Carrington, 2001), virus-encoded silencing suppressor constructs, or empty vector sequences. The concentration of each component was as follows: 35S:miR171 OD₆₀₀ = 0.75; 35S:SCL6-IV, OD₆₀₀ = 0.10; RNA silencing suppressors, OD₆₀₀ = 0.15; empty vector OD₆₀₀ = variable. Infiltrated leaves were harvested 48 h after injection, total RNA was extracted and 10 µg used for RNA gel blotting. SCL6-IV mRNA and its corresponding 3' cleavage product were detected by RNA gel blot assays with a ³²P-labeled DNA probe corresponding to the 3' end of SCL6-IV. Hybridization intensities were quantified using an Instant Imager (Molecular Dynamics) and exposures in the linear range of detection.

Virus Propagation and Inoculum Enrichment

Both TuMV-GFP and TuMV-AS9-GFP were propagated in *N. benthamiana*. TuMV-GFP infection was launched by inoculation with *Agrobacterium* containing pCB-TuMV-GFP, and systemically infected leaves were collected 13 DAI. TuMV-AS9-GFP infection was launched by coinjection of leaves with pCB-TuMV-AS9-GFP and p19-HA (Chapman et al., 2004), and injected leaves were harvested 5 DAI (Figure 2C). Virus preparations for subsequent inoculum were prepared using a polyethylene glycol precipitation procedure essentially as described (Choi et al., 1977) (see Supplemental Figure 1 online). The virus-enriched pellets were resuspended in 50 mM potassium phosphate, pH 7.5, and stored in 40% glycerol at -20°C.

Virus Infection Assays

Four *Arabidopsis* rosette leaves were dusted with carborundum and rub-inoculated using 3 µL of inoculum/leaf. In all experiments, inoculum levels were adjusted to levels at least fivefold higher than needed to achieve 100% systemic infection efficiency by TuMV-AS9-GFP in *dcl2-1 dcl3-1 dcl4-2* mutant plants, based on inoculum titration assays (see Supplemental Figure 1 online). Control plants were dusted with carborundum and mock-inoculated using 50 mM potassium phosphate, pH 7.5. Local and systemic infection of *Arabidopsis* by TuMV-GFP or TuMV-AS9-GFP was scored initially by GFP fluorescence. TuMV CP was detected by immunoblotting and chemiluminescence using antibody PVAS-134 at a 1:5000 dilution (Lellis et al., 2002) and Western Lighting plus-ECL substrate (Perkin-Elmer). Blots were exposed to film for 10, 30, 60, and 180 s to ensure signal detection in linear range. Four inoculated rosette leaves/plant were collected at 7 DAI and pooled into a single sample. From the same plants at later time points, four cauline leaves or four inflorescence clusters were pooled. In all experiments, four replicate samples were analyzed for each virus-plant genotype combination at each time point and for each tissue type. Total protein extracts were adjusted to 1.0 mg/mL prior to dilution for blot assays using 6.5 µg of total protein. The linear range of detection was between 0.5 and 12.6 µg of total protein for TuMV-AS9-GFP-infected *dcl2-1 dcl3-1 dcl4-2* triple mutant plants.

RNA Extraction and Small RNA Gel Blot Analysis

Total RNA was extracted using Trizol (Invitrogen) from whole individual plants or from independent pools of four inoculated rosette leaves, four noninoculated cauline leaves, or four inflorescence clusters. Blot hybridization was done as described (Llave et al., 2002a). ³²P-radiolabeled probes corresponding to the coding region for CI protein were generated by random priming of a PCR fragment [primers CI-F d(ACTCTCAATGATATAGAGGATG) and CI-R d(TTGATGGTGAAGCTGCCTCAAG)] using

pCB-TuMV as template. Blots were stripped and reprobed for endogenous RDR2/DCL3-dependent siRNA02, RDR6/DCL1/DCL4-dependent TAS1 tasiRNA 255, and U6 RNA using cDNA oligonucleotides end-labeled with [γ - 32 P]ATP using Optikinase (USB). Hybridization intensities were quantified as described for the transient assays and normalized to the U6 RNA signal.

Profiling TuMV-Derived siRNAs by High-Throughput Sequencing

Small RNA libraries from TuMV-infected or mock-inoculated plants were generated using sequencing-by-synthesis technology (Illumina Genome Analyzer I) (Fahlgren et al., 2009) and analyzed as described (Fahlgren et al., 2009). Bar-coded 5' adaptors (Cuperus et al., 2010) were used for multiplexing purposes. For each treatment, small RNA libraries were made independently from triplicate samples using 100 mg of total RNA extracted from aerial tissue from three plants. Four sets of amplicons were prepared using different bar-coded adaptors and were mixed in equal amounts (0.83 pMol/amplicon) and sequenced simultaneously in one lane. Small RNA sequences were parsed, and *Arabidopsis* and TuMV reads were identified, mapped, and quantified using CASHX (Fahlgren et al., 2009). Reads were normalized per 1,000,000 total reads.

Accession Number

Sequence data from this article can be found in Gene Expression Omnibus (<http://www.ncbi.nlm.nih.gov/geo>) under accession number GSE20197.

Supplemental Data

The following materials are available in the online version of this article.

Supplemental Figure 1. Enrichment and Titration of TuMV-AS9-GFP from *N. benthamiana*.

Supplemental Figure 2. Genome-Wide Profile of 21-Nucleotide Virus-Derived sRNAs in TuMV-Infected *Arabidopsis* Plants at 7 DAI.

Supplemental Figure 3. Genome-Wide Profile of 22-Nucleotide Virus-Derived sRNAs in TuMV-Infected *Arabidopsis* Plants at 7 DAI.

Supplemental Figure 4. Genome-Wide Profile of 22-Nucleotide Virus-Derived sRNAs in TuMV-Infected *Arabidopsis* Plants at 10 DAI.

Supplemental Figure 5. Accumulation of Antisense siRNAs Derived from the 5' UTR of TuMV-GFP in Inflorescence Clusters of *Arabidopsis dcl* and *rdr* Mutants.

Supplemental Figure 6. Strand and Nucleotide Bias of TuMV-Derived sRNAs.

Supplemental Figure 7. Accumulation of TuMV-GFP and TuMV-AS9-GFP in *Arabidopsis dcl* Mutants.

Supplemental Figure 8. Accumulation of TuMV-GFP and TuMV-AS9-GFP in *Arabidopsis rdr* Mutants.

Supplemental Table 1. Abundance and Distribution of 21-Nucleotide TuMV-Derived siRNA in Whole *Arabidopsis* Plants at 7 and 10 DAI.

Supplemental Methods. DNA Plasmids and Constructs.

ACKNOWLEDGMENTS

We thank members of the Carrington Lab for fruitful discussions and suggestions, Kristin Kasschau for technical assistance in making the small RNA libraries, and Nicholas Lowery for assistance with RNA extraction and analysis. H.G.-R. was supported by a Helen Hay Whitney postdoctoral fellowship (F-972). This work was supported by National Institutes of Health Grant A143288 and National Science Foundation Grant MCB-0618433 to J.C.C.

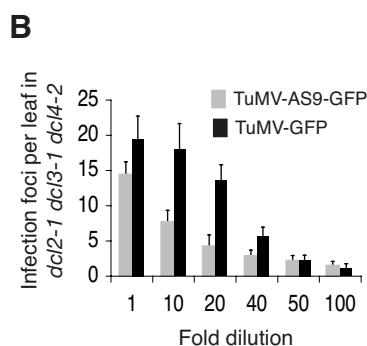
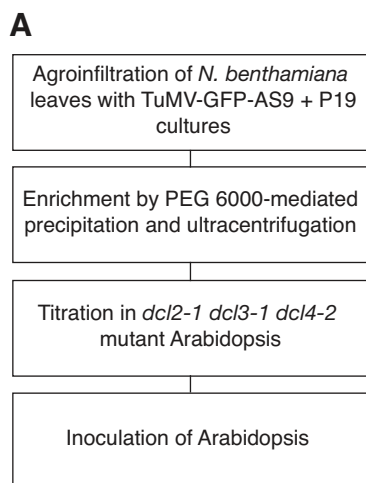
Received November 24, 2009; revised February 8, 2010; accepted February 15, 2010; published February 26, 2010.

REFERENCES

- Aliyari, R., Wu, Q., Li, H.W., Wang, X.H., Li, F., Green, L.D., Han, C.S., Li, W.X., and Ding, S.W. (2008). Mechanism of induction and suppression of antiviral immunity directed by virus-derived small RNAs in *Drosophila*. *Cell Host Microbe* **4**: 387–397.
- Allen, E., Xie, Z., Gustafson, A.M., and Carrington, J.C. (2005). MicroRNA-directed phasing during trans-acting siRNA biogenesis in plants. *Cell* **121**: 207–221.
- Allen, E., Xie, Z., Gustafson, A.M., Sung, G.H., Spatafora, J.W., and Carrington, J.C. (2004). Evolution of microRNA genes by inverted duplication of target gene sequences in *Arabidopsis thaliana*. *Nat. Genet.* **36**: 1282–1290.
- Baumberger, N., and Baulcombe, D.C. (2005). *Arabidopsis* ARGONAUTE1 is an RNA slicer that selectively recruits microRNAs and short interfering RNAs. *Proc. Natl. Acad. Sci. USA* **102**: 11928–11933.
- Blevins, T., Rajeswaran, R., Shivaprasad, P.V., Beknazariants, D., Si-Ammour, A., Park, H.S., Vazquez, F., Robertson, D., Meins, F., Jr., Hohn, T., and Pooggin, M.M. (2006). Four plant Dicers mediate viral small RNA biogenesis and DNA virus induced silencing. *Nucleic Acids Res.* **34**: 6233–6246.
- Borsani, O., Zhu, J., Verslues, P.E., Sunkar, R., and Zhu, J.K. (2005). Endogenous siRNAs derived from a pair of natural cis-antisense transcripts regulate salt tolerance in *Arabidopsis*. *Cell* **123**: 1279–1291.
- Bouche, N., Laressergues, D., Gascioli, V., and Vaucheret, H. (2006). An antagonistic function for *Arabidopsis* DCL2 in development and a new function for DCL4 in generating viral siRNAs. *EMBO J.* **25**: 3347–3356.
- Cao, X., and Jacobsen, S.E. (2002). Role of the *Arabidopsis* DRM methyltransferases in de novo DNA methylation and gene silencing. *Curr. Biol.* **12**: 1138–1144.
- Chapman, E.J., Prokhnevsky, A.I., Gopinath, K., Dolja, V.V., and Carrington, J.C. (2004). Viral RNA silencing suppressors inhibit the microRNA pathway at an intermediate step. *Genes Dev.* **18**: 1179–1186.
- Choi, J.K., Maeda, T., and Wakimoto, S. (1977). An improved method for purification of Turnip mosaic virus. *Ann. Phytopath. Soc. Japan* **43**: 440–448.
- Cuperus, J.T., Montgomery, T.A., Fahlgren, N., Burke, R.T., Townsend, T., Sullivan, C.M., and Carrington, J.C. (2010). Identification of MIR390a precursor processing-defective mutants in *Arabidopsis* by direct genome sequencing. *Proc. Natl. Acad. Sci. USA* **107**: 466–471.
- Dalmay, T., Hamilton, A., Rudd, S., Angell, S., and Baulcombe, D.C. (2000). An RNA-dependent RNA polymerase gene in *Arabidopsis* is required for posttranscriptional gene silencing mediated by a transgene but not by a virus. *Cell* **101**: 543–553.
- Deleris, A., Gallego-Bartolome, J., Bao, J., Kasschau, K.D., Carrington, J.C., and Voinnet, O. (2006). Hierarchical action and inhibition of plant Dicer-like proteins in antiviral defense. *Science* **313**: 68–71.
- Diaz-Pendon, J.A., Li, F., Li, W.X., and Ding, S.W. (2007). Suppression of antiviral silencing by cucumber mosaic virus 2b protein in *Arabidopsis* is associated with drastically reduced accumulation of three classes of viral small interfering RNAs. *Plant Cell* **19**: 2053–2063.
- Ding, S.W., and Voinnet, O. (2007). Antiviral immunity directed by small RNAs. *Cell* **130**: 413–426.
- Donaire, L., Barajas, D., Martinez-Garcia, B., Martinez-Priego, L.,

- Pagan, I., and Llave, C. (2008). Structural and genetic requirements for the biogenesis of tobacco rattle virus-derived small interfering RNAs. *J. Virol.* **82**: 5167–5177.
- Donaire, L., Wang, Y., Gonzalez-Ibeas, D., Mayer, K.F., Aranda, M.A., and Llave, C. (2009). Deep-sequencing of plant viral small RNAs reveals effective and widespread targeting of viral genomes. *Virology* **392**: 203–214.
- Dong, Z., Han, M.H., and Fedoroff, N. (2008). The RNA-binding proteins HYL1 and SE promote accurate in vitro processing of pri-miRNA by DCL1. *Proc. Natl. Acad. Sci. USA* **105**: 9970–9975.
- Fahlgren, N., Sullivan, C.M., Kasschau, K.D., Chapman, E.J., Cumbie, J.S., Montgomery, T.A., Gilbert, S.D., Dasenko, M., Backman, T.W., Givan, S.A., and Carrington, J.C. (2009). Computational and analytical framework for small RNA profiling by high-throughput sequencing. *RNA* **15**: 992–1002.
- Flynt, A., Liu, N., Martin, R., and Lai, E.C. (2009). Dicing of viral replication intermediates during silencing of latent Drosophila viruses. *Proc. Natl. Acad. Sci. USA* **106**: 5270–5275.
- Fusaro, A.F., Matthew, L., Smith, N.A., Curtin, S.J., Dedic-Hagan, J., Ellacott, G.A., Watson, J.M., Wang, M.B., Brosnan, C., Carroll, B.J., and Waterhouse, P.M. (2006). RNA interference-inducing hairpin RNAs in plants act through the viral defence pathway. *EMBO Rep.* **7**: 1168–1175.
- Garcia-Ruiz, H., and Ahlquist, P. (2006). Inducible yeast system for Viral RNA recombination reveals requirement for an RNA replication signal on both parental RNAs. *J. Virol.* **80**: 8316–8328.
- Gascioli, V., Mallory, A.C., Bartel, D.P., and Vaucheret, H. (2005). Partially redundant functions of *Arabidopsis* DICER-like enzymes and a role for DCL4 in producing trans-acting siRNAs. *Curr. Biol.* **15**: 1494–1500.
- Grigg, S.P., Canales, C., Hay, A., and Tsiantis, M. (2005). SERRATE coordinates shoot meristem function and leaf axial patterning in *Arabidopsis*. *Nature* **437**: 1022–1026.
- Han, M.H., Goud, S., Song, L., and Fedoroff, N. (2004). The *Arabidopsis* double-stranded RNA-binding protein HYL1 plays a role in microRNA-mediated gene regulation. *Proc. Natl. Acad. Sci. USA* **101**: 1093–1098.
- Ji, L.H., and Ding, S.W. (2001). The suppressor of transgene RNA silencing encoded by Cucumber mosaic virus interferes with salicylic acid-mediated virus resistance. *Mol. Plant Microbe Interact.* **14**: 715–724.
- Johansen, L.K., and Carrington, J.C. (2001). Silencing on the spot: induction and suppression of RNA silencing in the *Agrobacterium*-mediated transient expression system. *Plant Physiol.* **126**: 930–938.
- Kasschau, K.D., and Carrington, J.C. (2001). Long-distance movement and replication maintenance functions correlate with silencing suppression activity of potyviral HC-Pro. *Virology* **285**: 71–81.
- Kasschau, K.D., Cronin, S., and Carrington, J.C. (1997). Genome amplification and long-distance movement functions associated with the central domain of tobacco etch potyvirus helper component-proteinase. *Virology* **228**: 251–262.
- Kasschau, K.D., Xie, Z., Allen, E., Llave, C., Chapman, E.J., Krizan, K.A., and Carrington, J.C. (2003). P1/HC-Pro, a viral suppressor of RNA silencing, interferes with *Arabidopsis* development and miRNA function. *Dev. Cell* **4**: 205–217.
- Lakatos, L., Csorba, T., Pantaleo, V., Chapman, E.J., Carrington, J.C., Liu, Y.P., Dolja, V.V., Calvino, L.F., Lopez-Moya, J.J., and Burgyan, J. (2006). Small RNA binding is a common strategy to suppress RNA silencing by several viral suppressors. *EMBO J.* **25**: 2768–2780.
- Lellis, A.D., Kasschau, K.D., Whitham, S.A., and Carrington, J.C. (2002). Loss-of-susceptibility mutants of *Arabidopsis thaliana* reveal an essential role for eIF(iso)4E during potyvirus infection. *Curr. Biol.* **12**: 1046–1051.
- Li, C.F., Pontes, O., El-Shami, M., Henderson, I.R., Bernatavichute, Y.V., Chan, S.W., Lagrange, T., Pikaard, C.S., and Jacobsen, S.E. (2006). An ARGONAUTE4-containing nuclear processing center colocalized with Cajal bodies in *Arabidopsis thaliana*. *Cell* **126**: 93–106.
- Llave, C., Kasschau, K.D., Rector, M.A., and Carrington, J.C. (2002b). Endogenous and silencing-associated small RNAs in plants. *Plant Cell* **14**: 1605–1619.
- Llave, C., Xie, Z., Kasschau, K.D., and Carrington, J.C. (2002a). Cleavage of Scarecrow-like mRNA targets directed by a class of *Arabidopsis* miRNA. *Science* **297**: 2053–2056.
- Meyers, B.C., et al. (2008). Criteria for annotation of plant microRNAs. *Plant Cell* **20**: 3186–3190.
- Mi, S., et al. (2008). Sorting of small RNAs into *Arabidopsis* argonaute complexes is directed by the 5' terminal nucleotide. *Cell* **133**: 116–127.
- Mlotshwa, S., Pruss, G.J., Peragine, A., Endres, M.W., Li, J., Chen, X., Poethig, R.S., Bowman, L.H., and Vance, V. (2008). DICER-LIKE2 plays a primary role in transitive silencing of transgenes in *Arabidopsis*. *PLoS One* **3**: e1755.
- Moissiard, G., and Voinnet, O. (2006). RNA silencing of host transcripts by cauliflower mosaic virus requires coordinated action of the four *Arabidopsis* Dicer-like proteins. *Proc. Natl. Acad. Sci. USA* **103**: 19593–19598.
- Molnar, A., Csorba, T., Lakatos, L., Varallyay, E., Lacomme, C., and Burgyan, J. (2005). Plant virus-derived small interfering RNAs originate predominantly from highly structured single-stranded viral RNAs. *J. Virol.* **79**: 7812–7818.
- Montgomery, T.A., Howell, M.D., Cuperus, J.T., Li, D., Hansen, J.E., Alexander, A.L., Chapman, E.J., Fahlgren, N., Allen, E., and Carrington, J.C. (2008a). Specificity of ARGONAUTE7-miR390 interaction and dual functionality in TAS3 trans-acting siRNA formation. *Cell* **133**: 128–141.
- Montgomery, T.A., Yoo, S.J., Fahlgren, N., Gilbert, S.D., Howell, M. D., Sullivan, C.M., Alexander, A., Nguyen, G., Allen, E., Ahn, J.H., and Carrington, J.C. (2008b). AGO1-miR173 complex initiates phased siRNA formation in plants. *Proc. Natl. Acad. Sci. USA* **105**: 20055–20062.
- Mourrain, P., et al. (2000). *Arabidopsis* SGS2 and SGS3 genes are required for posttranscriptional gene silencing and natural virus resistance. *Cell* **101**: 533–542.
- Park, W., Li, J., Song, R., Messing, J., and Chen, X. (2002). CARPEL FACTORY, a Dicer homolog, and HEN1, a novel protein, act in microRNA metabolism in *Arabidopsis thaliana*. *Curr. Biol.* **12**: 1484–1495.
- Peragine, A., Yoshikawa, M., Wu, G., Albrecht, H.L., and Poethig, R.S. (2004). SGS3 and SGS2/SDE1/RDR6 are required for juvenile development and the production of trans-acting siRNAs in *Arabidopsis*. *Genes Dev.* **18**: 2368–2379.
- Pontes, O., Li, C.F., Nunes, P.C., Haag, J., Ream, T., Vitins, A., Jacobsen, S.E., and Pikaard, C.S. (2006). The *Arabidopsis* chromatin-modifying nuclear siRNA pathway involves a nucleolar RNA processing center. *Cell* **126**: 79–92.
- Qi, X., Bao, F.S., and Xie, Z. (2009). Small RNA deep sequencing reveals role for *Arabidopsis thaliana* RNA-dependent RNA polymerases in viral siRNA biogenesis. *PLoS One* **4**: e4971.
- Qi, Y., He, X., Wang, X.J., Kohany, O., Jurka, J., and Hannon, G.J. (2006). Distinct catalytic and non-catalytic roles of ARGONAUTE4 in RNA-directed DNA methylation. *Nature* **443**: 1008–1012.
- Qu, F., Ye, X., Hou, G., Sato, S., Clemente, T.E., and Morris, T.J. (2005). RDR6 has a broad-spectrum but temperature-dependent antiviral defense role in *Nicotiana benthamiana*. *J. Virol.* **79**: 15209–15217.

- Qu, F., Ye, X., and Morris, T.J.** (2008). *Arabidopsis* DRB4, AGO1, AGO7, and RDR6 participate in a DCL4-initiated antiviral RNA silencing pathway negatively regulated by DCL1. *Proc. Natl. Acad. Sci. USA* **105**: 14732–14737.
- Reinhart, B.J., Weinstein, E.G., Rhoades, M.W., Bartel, B., and Bartel, D.P.** (2002). MicroRNAs in plants. *Genes Dev.* **16**: 1616–1626.
- Schmid, M., Davison, T.S., Henz, S.R., Pape, U.J., Demar, M., Vingron, M., Scholkopf, B., Weigel, D., and Lohmann, J.U.** (2005). A gene expression map of *Arabidopsis thaliana* development. *Nat. Genet.* **37**: 501–506.
- Schwach, F., Vaistij, F.E., Jones, L., and Baulcombe, D.C.** (2005). An RNA-dependent RNA polymerase prevents meristem invasion by potato virus X and is required for the activity but not the production of a systemic silencing signal. *Plant Physiol.* **138**: 1842–1852.
- Vaucheret, H., Vazquez, F., Crete, P., and Bartel, D.P.** (2004). The action of ARGONAUTE1 in the miRNA pathway and its regulation by the miRNA pathway are crucial for plant development. *Genes Dev.* **18**: 1187–1197.
- Vazquez, F., Vaucheret, H., Rajagopalan, R., Lepers, C., Gascioli, V., Mallory, A.C., Hilbert, J.L., Bartel, D.P., and Crete, P.** (2004). Endogenous trans-acting siRNAs regulate the accumulation of *Arabidopsis* mRNAs. *Mol. Cell* **16**: 69–79.
- Voinnet, O.** (2005). Non-cell autonomous RNA silencing. *FEBS Lett.* **579**: 5858–5871.
- Wang, X.B., Wu, Q., Ito, T., Cillo, F., Li, W.X., Chen, X., Yu, J.L., and Ding, S.W.** (2010). RNAi-mediated viral immunity requires amplification of virus-derived siRNAs in *Arabidopsis thaliana*. *Proc. Natl. Acad. Sci. USA* **107**: 484–489.
- Wierzbicki, A.T., Ream, T.S., Haag, J.R., and Pikaard, C.S.** (2009). RNA polymerase V transcription guides ARGONAUTE4 to chromatin. *Nat. Genet.* **41**: 630–634.
- Xie, Z., Allen, E., Wilken, A., and Carrington, J.C.** (2005). DICER-LIKE 4 functions in trans-acting small interfering RNA biogenesis and vegetative phase change in *Arabidopsis thaliana*. *Proc. Natl. Acad. Sci. USA* **102**: 12984–12989.
- Xie, Z., Fan, B., Chen, C., and Chen, Z.** (2001). An important role of an inducible RNA-dependent RNA polymerase in plant antiviral defense. *Proc. Natl. Acad. Sci. USA* **98**: 6516–6521.
- Xie, Z., Johansen, L.K., Gustafson, A.M., Kasschau, K.D., Lellis, A.D., Zilberman, D., Jacobsen, S.E., and Carrington, J.C.** (2004). Genetic and functional diversification of small RNA pathways in plants. *PLoS Biol.* **2**: E104.
- Yang, S.J., Carter, S.A., Cole, A.B., Cheng, N.H., and Nelson, R.S.** (2004). A natural variant of a host RNA-dependent RNA polymerase is associated with increased susceptibility to viruses by *Nicotiana benthamiana*. *Proc. Natl. Acad. Sci. USA* **101**: 6297–6302.
- Yoshikawa, M., Peragine, A., Park, M.Y., and Poethig, R.S.** (2005). A pathway for the biogenesis of trans-acting siRNAs in *Arabidopsis*. *Genes Dev.* **19**: 2164–2175.
- Yu, D., Fan, B., MacFarlane, S.A., and Chen, Z.** (2003). Analysis of the involvement of an inducible *Arabidopsis* RNA-dependent RNA polymerase in antiviral defense. *Mol. Plant Microbe Interact.* **16**: 206–216.
- Zilberman, D., Cao, X., and Jacobsen, S.E.** (2003). ARGONAUTE4 control of locus-specific siRNA accumulation and DNA and histone methylation. *Science* **299**: 716–719.

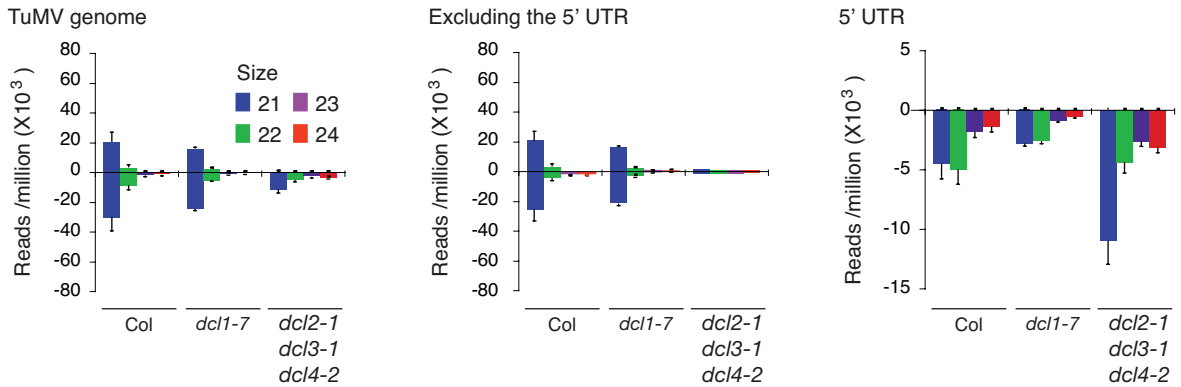


Supplemental Figure 1. Enrichment and titration of TuMV-AS9-GFP from *N. benthamiana*.

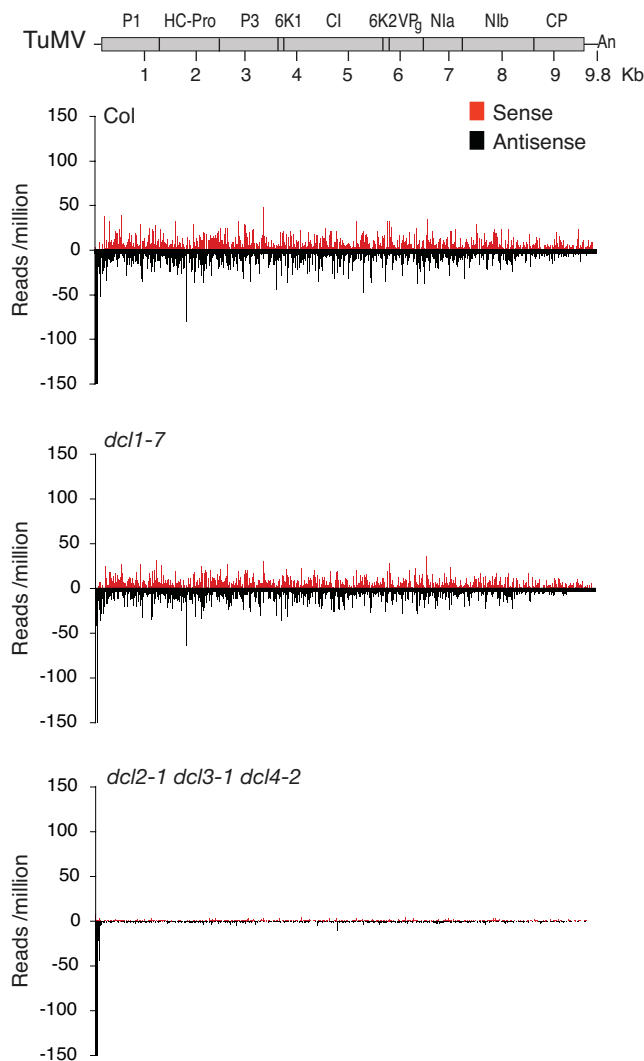
(A) Leaves were infiltrated with *Agrobacterium* cultures transformed with p19-HA or pCB-TuMV-AS9-GFP, each at OD₆₀₀=0.5. Infiltrated leaves were collected at 5 DAI. Parental TuMV-GFP was propagated in *N. benthamiana* infiltrated with *Agrobacterium* transformed with pCB-TuMV-GFP, and systemically infected leaves collected at 13 DAI. Fresh TuMV-AS9-GFP or TuMV-GFP infected tissue was blended and the inoculum enriched by PEG 600-mediated precipitation and ultracentrifugation.

(B) Enriched inoculum resuspended in 50 mM potassium phosphate was stored at -20°C in 40% glycerol. Enriched inoculum was titrated using *dcl2-1 dcl3-2 dcl4-2* triple mutant Arabidopsis. Four leaves per plant were inoculated with 3 µl each. Inoculum strength was measured as the number of infection foci per leaf. The histogram shows the average and standard error for twenty-four leaves per dilution.

A TuMV-derived siRNA abundance at 7 DAI



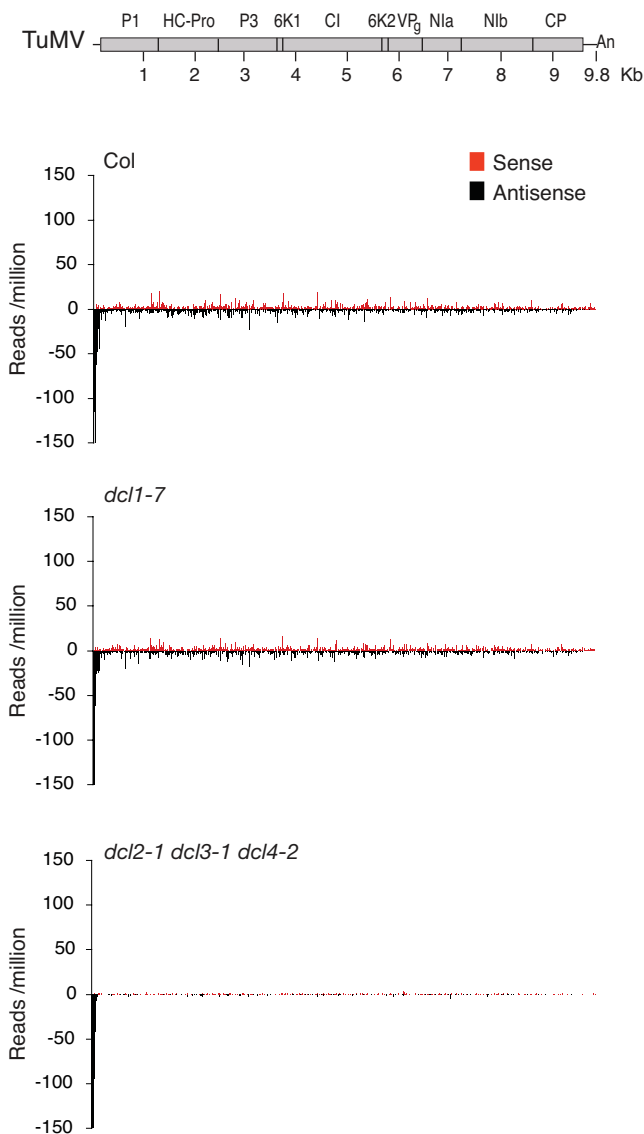
B Genome-wide distribution of 21-nt sRNAs at 7 DAI



Supplemental Figure 2. Genome-wide profile of 21-nt TuMV-derived siRNAs in infected *Arabidopsis* plants at 7 DAI.

Values are averages and standard error from three replicate libraries, normalized to (*Arabidopsis* plus TuMV) reads per million. Sense- and antisense-polarity reads were plotted on the y-axis in the positive and negative directions, respectively. (A) Abundance, by size class and polarity, of siRNAs derived from TuMV, its 5' UTR or the rest of the genome. (B) Genome-wide distribution of 21-nt virus-derived siRNAs on the sense and antisense strands of TuMV. The scale was capped at 150.

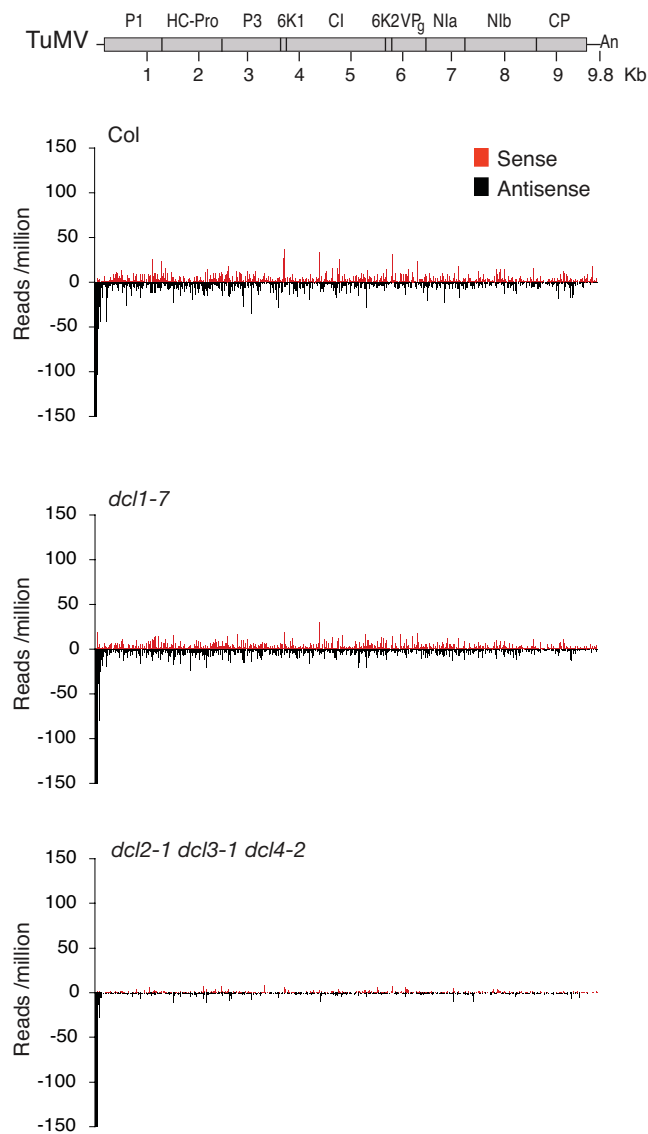
TuMV genome-wide distribution of 22-nt sRNAs at 7 DAI



Supplemental Figure 3. Genome-wide profile of 22-nt long virus-derived siRNAs in TuMV-infected *Arabidopsis* plants at 7 DAI.

Values are averages and standard error from three replicate libraries, normalized to (*Arabidopsis* plus TuMV) reads per million. Sense- and antisense-polarity reads were plotted on the y-axis in the positive and negative directions, respectively. Scale was capped at 150 reads.

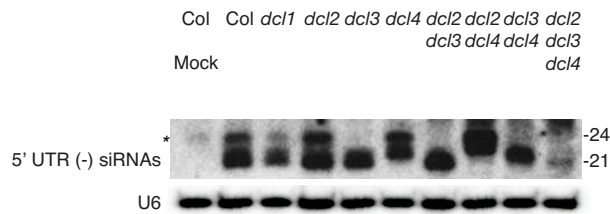
TuMV genome-wide distribution of 22-nt sRNAs at 10 DAI



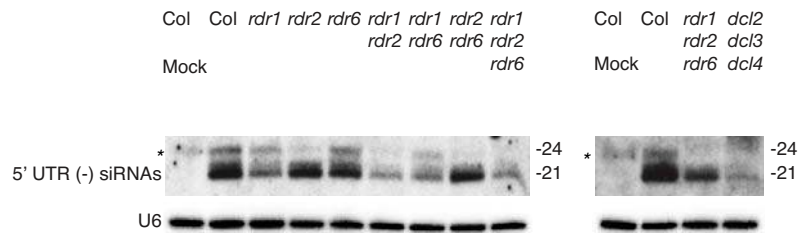
Supplemental Figure 4. Genome-wide profile of 22-nt long virus-derived siRNAs in TuMV-infected *Arabidopsis* plants at 10 DAI.

Values are averages and standard error from three replicate libraries, normalized to (*Arabidopsis* plus TuMV) reads per million. Sense- and antisense-polarity reads were plotted on the y-axis in the positive and negative directions, respectively. Scale was capped at 150 reads.

A *Arabidopsis dcl* mutants at 15 DAI



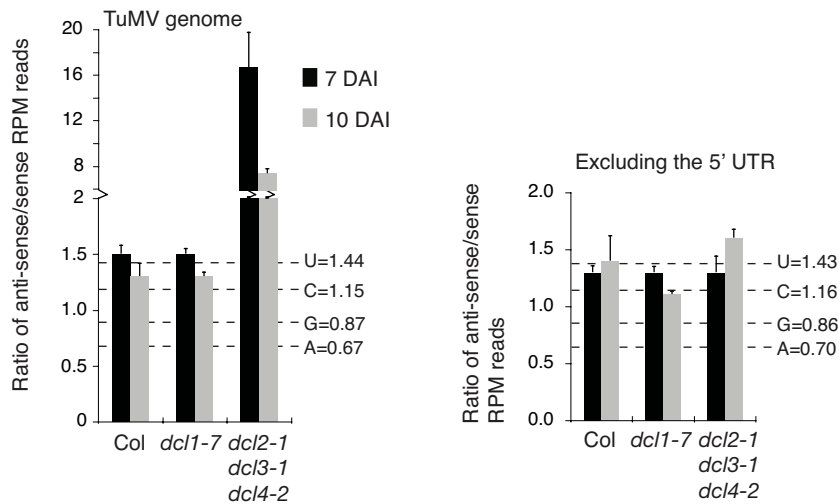
B *Arabidopsis rdr* mutants at 15 DAI



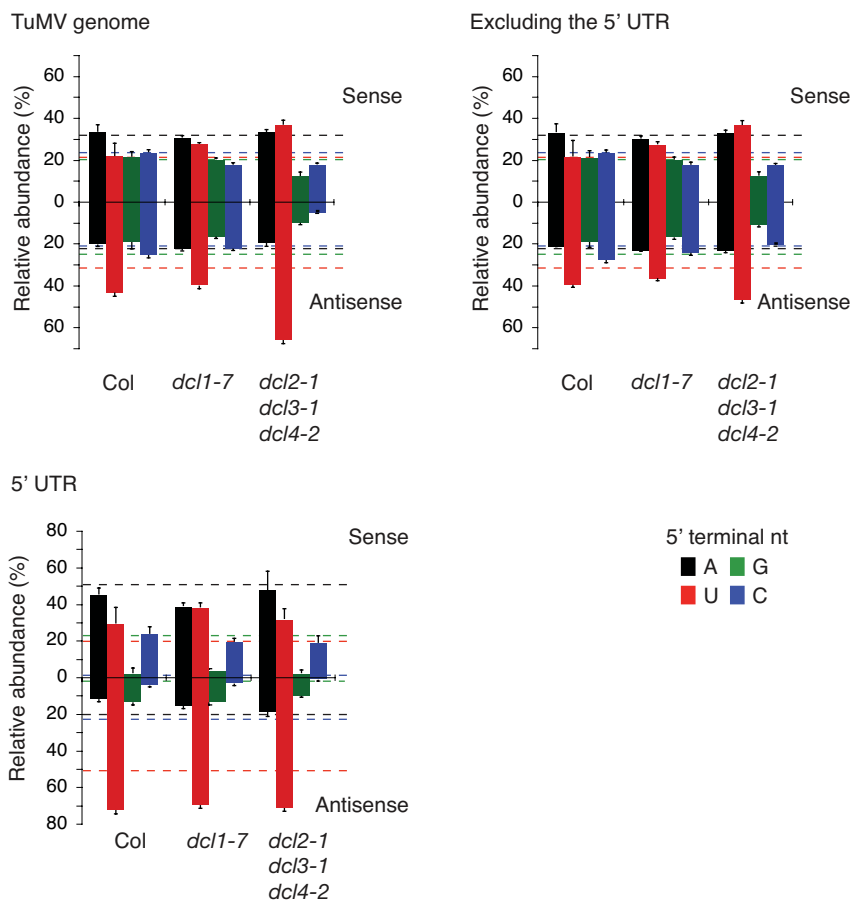
Supplemental Figure 5. Accumulation of antisense siRNAs derived from the 5' UTR of TuMV-GFP in inflorescence clusters of *Arabidopsis dcl* (A) and *rdr* (B) mutants.

For the samples described in Fig. 6C and 8C, accumulation of antisense siRNAs derived from the 5' UTR was determined by Northern blotting. siRNAs were detected using a mixture of four overlapping 42-nt long oligos spanning the entire 5' UTR and end-labeled with ³²P-ATP. U6 is indicated as a loading control. The asterisk indicates a background 24-nt long sRNA detected in mock inoculated Col-0 and other genotypes in a DCL3- and RDR2-dependent manner.

A Strand bias of 21-nt virus-derived sRNAs

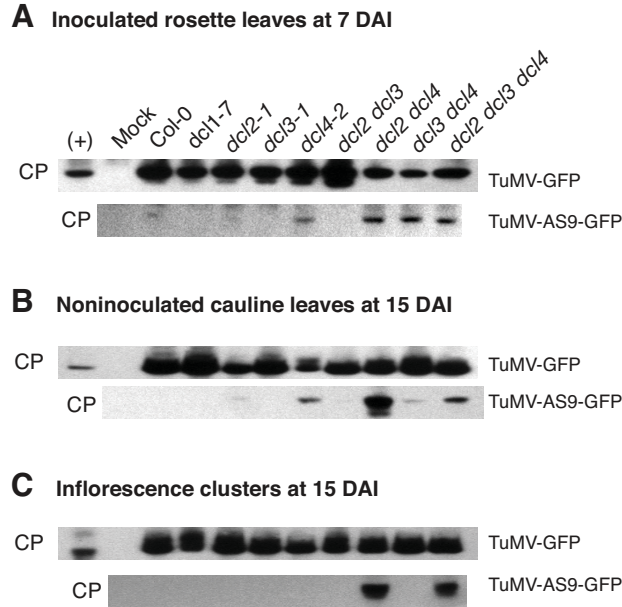


B Abundance of 21-nt sRNAs by 5' terminal nucleotide, at 10 DAI



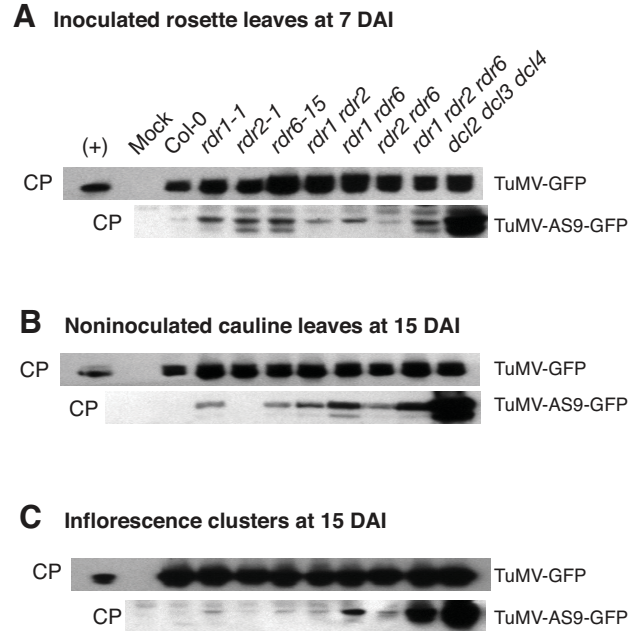
Supplemental Figure 6. Strand and nucleotide bias of TuMV-derived siRNAs.

(A) Strand bias of 21-nt long virus-derived siRNAs obtained at 7 and 10 DAI, measured as the ratio of antisense to sense reads per genotype and time point. The histogram shows the average and standard error of three replicate libraries for RPM normalized reads mapping to the entire TuMV genome (left panel), or excluding the 5' UTR (right panel). Dashed horizontal lines indicate the values expected from the nucleotide composition of the TuMV genome (antisense/ sense). (B) Relative abundance by polarity and 5' terminal nucleotide of 21-nt long virus-derived siRNAs mapping to the entire TuMV genome, the 5' UTR, or the rest of the genome, in the libraries made from TuMV infected plants at 10 DAI. Dashed, horizontal colored lines indicate the values expected from the TuMV nucleotide composition (sense or antisense).



Supplemental Figure 7. Accumulation of TuMV-GFP and TuMV-AS-GFP in *Arabidopsis dcl* mutants.

Coat protein (CP) was detected by immunoblotting using antibody PVAS-134. For each virus-plant genotype combination, at each time point and for each tissue type, four replicates samples were analyzed using 6.25 micrograms of total protein and exposing to film several times. Representative blots are shown. In blots containing TuMV-GFP, TuMV-AS9-GFP in *dcl2-1 dcl3-1 dcl4-2* was included as normalization control. (A) Inoculated leaves. (B) Noninoculated cauline leaves. (C) Inflorescence. (+) indicates *dcl2-1 dcl3-1 dcl4-2* plants infected by TuMV-AS9-GFP, for comparison.



Supplemental Figure 8. Accumulation of TuMV-GFP and TuMV-AS-GFP in *Arabidopsis rdr* mutants.

Coat protein (CP) was detected by immunoblotting using antibody PVAS-134. For each virus-plant genotype combination, at each time point and for each tissue type, four replicates samples were analyzed using 6.25 micrograms of total protein and exposing to film several times. Representative blots are shown. In blots containing TuMV-GFP, TuMV-AS9-GFP in *dcl2-1 dcl3-1 dcl4-2* was included as normalization control. (A) Inoculated leaves. (B) Noninoculated cauline leaves. (C) Inflorescence. (+) indicates *dcl2-1 dcl3-1 dcl4-2* plants infected by TuMV-AS9-GFP, for comparison.

Supplemental Table 1. Abundance and distribution of 21 nt TuMV-derived siRNA in whole *Arabidopsis* plants at 7 and 10 DAI ^a.

Genotype	Time point	TuMV genome			5' UTR		Excluding the 5' UTR	
		Total	Sense	Antisense	Sense	Antisense	Sense	Antisense
Col-0	7 DAI	50,617 (100%)	20,503 (40.5%)	30,114 (59.5%)	55 (0.1%)	4,541 (9.0%)	20,448 (40.4%)	25,573 (50.5%)
	10 DAI	108,591 (100%)	45,297 (41.7%)	63,294 (58.3%)	68 (0.1%)	8,031 (7.4%)	45,229 (41.7%)	55,263 (50.9%)
<i>dcl1-7</i>	7 DAI	39,981 (100%)	15,968 (39.9%)	24,013 (60.1%)	47 (0.1%)	2,790 (7.0%)	15,921 (39.8%)	21,222 (53.1%)
	10 DAI	80,637 (100%)	35,885 (44.5%)	44,752 (55.5%)	128 (0.2%)	5,100 (6.3%)	35,756 (44.3%)	39,652 (49.2%)
<i>dcl2-1</i>	7 DAI	11,614 (100%)	609 (5.2%)	11,005 (94.8%)	20 (0.2%)	10,956 (94.3%)	589 (5.1%)	49 (0.4%)
<i>dcl3-1</i> <i>dcl4-2</i>	10 DAI	15,891 (100%)	1,746 (11.0%)	14,144 (89.0%)	19 (0.1%)	11,862 (74.6%)	1,728 (10.9%)	2,283 (14.4%)

^a Average number of reads obtained in three replicate libraries per treatment, normalized to reads per million (*Arabidopsis* plus TuMV reads). Numbers in parenthesis are the relative abundance, in percentage, of TuMV-derived sRNA reads with respect to the total. This table is a numeric summary of the data presented in Figure 4 and Supplemental Figure 2.

SUPPLEMENTAL METHODS

Garcia-Ruiz et al. (2010). Plant Cell 10.1105/tpc.109.073056

DNA plasmids and constructs. Recombinant plasmids were constructed as follows.

pCBP1/HCPProHA-AS9. The TuMV HC-Pro sequence in pCBP1/HCPProHA-AS9 has the AS9 mutation, which leads to the same amino acid changes as the *Tobacco etch virus* AS9 mutation (Kasschau et al., 1997). Plasmid pCBP1/HCPProHA-AS9 was generated by site-directed mutagenesis of pCBP1/HCPProHA (Chapman et al., 2004) by using two sets of primers: Nco-HC-F d(ATCGCCATGGCAGCAGTTACATTTGCAACCGCTATCA) and AS9-R d(CGTGACCCATTTGGTGCAGCTGCTGTCTCGTATTGG); and AS9-F d(CCAATACGAGACAGCAGCTGCACCAAATGGGTCACG) and pCBXba-R d(GGTGATTTGCGGACTCTAGA). Then, a PCR fragment was amplified from these two PCR fragments by using Nco-HC-F and pCBXba-R. The NcoI-XbaI fragment was used to replace the NcoI-XbaI fragment of pCBP1/HCPProHA.

pCB-TuMV-GFP (Accession EF028235). Plasmid p35STuMV-GFP (Lellis et al., 2002) contains a TuMV cDNA cassette and sequence encoding a soluble-modified GFP between P1 and HC-Pro under control of the *Cauliflower mosaic virus* 35S promoter and Nos terminator (Sanchez et al., 1998). The SmaI-ApaI fragment of p35STuMV-GFP was inserted between SmaI and ApaI sites of pCB302 (Xiang et al., 1999), creating pCB-TuMV-GFP, a binary vector suitable for launching TuMV-GFP infection by *Agrobacterium* infiltration.

pCRGFP-HCPPro-AS9. Two PCR fragments were amplified from pCBTuMV-GFP by using two sets of primers: TuP1-ApaLI-F d(CGGTGACACAGAATATGCA) and TuHC-Eco57iR d(GTGAACCCTTCTCAATGT); and TuMV2579F d(CCATCTAGTGATTGGTAAC) and TuMV3490R d(AGAATGGCATGGTGG-AATGCAA). The third PCR fragment was amplified from pCBP1/HCPProHA-AS9 by using TuMV2124F d(AGCACGATACCTGAAGAAC) and HCgsR

d(CCTTGACATTTACCAACATGG). Then, a PCR fragment was amplified from these three PCR fragments by using TuP1-ApaLI-F and TuMV3490R. Such PCR fragment was inserted into pCR4zeroblunt TOPO vector (Invitrogen), creating pCRGFP-HCPro-AS9 which was used for making pCB-TuMV-AS9-GFP.

pCB-TuMV-AS9-GFP. The small NcoI-SnaBI fragment from pCRGFP-HCPro-AS9 was used to replace the NcoI-SnaBI fragment of pCB-TuMV-GFP.

pCB-TuMV. The small Stul-AgeI fragment from pCBP1/HCProHA (Chapman et al., 2004) was used to replace the equivalent Stul-AgeI fragment of pCB-TuMV-AS9-GFP.

pCB-TuMV-AS9. The small Stul-AgeI fragment from pCBP1/HCProHA-AS9 (Chapman et al., 2004) was used to replace the small Stul-AgeI fragment of pCB-TuMV-AS9-GFP.

Silencing suppressor constructs. P19-HA and p21-HA constructs were described previously (Chapman et al., 2004) and encoded HA-tagged versions of suppressors from *Tomato bushy stunt virus* and *Beet yellows virus*, respectively. Silencing suppression-defective mutants p19m (p19W39/42R) (Vargason et al., 2003) and described previously (Chiba et al., 2006) have been described previously.

SUPPLEMENTAL REFERENCES

- Chapman, E.J., Prokhnevsky, A.I., Gopinath, K., Dolja, V.V., and Carrington, J.C.** (2004). Viral RNA silencing suppressors inhibit the microRNA pathway at an intermediate step. *Genes Dev* **18**, 1179-1186.
- Chiba, M., Reed, J.C., Prokhnevsky, A.I., Chapman, E.J., Mawassi, M., Koonin, E.V., Carrington, J.C., and Dolja, V.V.** (2006). Diverse suppressors of RNA silencing enhance agroinfection by a viral replicon. *Virology* **346**, 7-14.
- Kasschau, K.D., Cronin, S., and Carrington, J.C.** (1997). Genome amplification and long-distance movement functions associated with the central domain of tobacco etch potyvirus helper component-proteinase. *Virology* **228**, 251-262.
- Lellis, A.D., Kasschau, K.D., Whitham, S.A., and Carrington, J.C.** (2002). Loss-of-susceptibility mutants of *Arabidopsis thaliana* reveal an essential role for eIF(iso)4E during potyvirus infection. *Curr. Biol.* **12**, 1046-1051.

- Sanchez, F., Martinez-Herrera, D., Aguilar, I., and Ponz, F.** (1998). Infectivity of turnip mosaic potyvirus cDNA clones and transcripts on the systemic host *Arabidopsis thaliana* and local lesion hosts. *Virus Res* **55**, 207-219.
- Vargason, J.M., Szittyá, G., Burgyan, J., and Tanaka Hall, T.M.** (2003). Size selective recognition of siRNA by an RNA silencing suppressor. *Cell* **115**, 799-811.
- Xiang, C., Han, P., Lutziger, I., Wang, K., and Oliver, D.J.** (1999). A mini binary vector series for plant transformation. *Plant Mol Biol* **40**, 711-717.